Development of a Multifunctional Dressing for Epidermal Wound Monitoring and On-Site Drug Delivery

by

Bahram Mirani
Bachelor of Science, K. N. Toosi University of Technology, 2008

A Thesis Submitted in Partial Fulfillment
of the Requirements for the Degree of

MASTER OF APPLIED SCIENCE

in the Department of Mechanical Engineering

Supervisory Committee

Development of a Multifunctional Dressing for Epidermal Wound Monitoring and On-Site Drug Delivery

by

Bahram Mirani
Bachelor of Science, K. N. Toosi University of Technology, 2008

Supervisory Committee

Dr. Mohsen Akbari, Department of Mechanical Engineering
Supervisor

Dr. Stephanie Willerth, Department of Mechanical Engineering
Departmental Member

Abstract

Supervisory Committee
Dr. Mohsen Akbari, Department of Mechanical Engineering
Supervisor
Dr. Stephanie Willerth, Department of Mechanical Engineering
Departmental Member

The treatment of epidermal wounds, particularly chronic wounds, is one of the most ubiquitous medical challenges and has imposed a considerable financial burden on the global health care system. Several factors in epidermal wounds lead to severe medical conditions among which infection comprises a large number of mortalities. To tackle this issue, great efforts have been made in the last decades to incorporate antimicrobial agents into wound dressings in order to inhibit microorganism colonization. Additionally, various wound monitoring systems have been developed to detect and track infections using different indicators such as bacterial by-products. However, the integration of these infection sensors with wound dressings – most of which have benefited from electrochemical detectors – has been a major bottleneck due to the electrode failure in the wound environment and the need for electrical power supply. Other approaches have focused on the development of point-of-care devices that simplify the detection of infection. This study aims to address the aforementioned challenge by developing a multifunctional hydrogel-based wound dressing – made of alginate 1.5% (w/v) – for on-site infection monitoring via colourimetric and image processing methods. Taking advantage of wound acidity as an indicator of bacterial infection, the developed wound dressing was composed of an array of pH sensors, fabricated by 3-dimensional (3D) bioprinting. Brilliant Yellow and cabbage juice as two pH responsive dyes were immobilized in the pH sensors to facilitate a wireless wound monitoring. In this system, Brilliant Yellow afforded a higher accuracy in image processing while cabbage juice provided a better visual observation of the wound condition. The functionality of the developed dressing in detecting bacterial infection was evaluated via an ex-vivo test on pig skin samples, infected by *Pseudomonas aeruginosa*, and the presence of bacteria was detected within 30 minutes after the placement of the dressings on the skin samples.

Moreover, the inclusion of gentamicin-loaded components into the wound dressing facilitated the inhibition of bacterial growth, which was evaluated in vitro on the same strain of bacteria. In this experiment, 2 mg/ml of gentamicin in the hydrogel led to the eradication of *P. aeruginosa*. This incorporation of antibiotic delivery along with the simple colourimetric infection detection holds a great promise for managing acute and chronic wounds by inhibition of bacterial growth and monitoring infection in real-time without a need for dressing removal.

Table of Contents

List of Tables

List of Figures

Acknowledgments

I would like to thank Dr. Mohsen Akbari for his continuous support and helpful guidance throughout my degree. He has always strengthened my motivation in research.

I am also grateful to Dr. Stephanie Willerth who provided me with a great support and kindly gave me the opportunity to use the facilities of her laboratory.

Special thanks go to Erik Pagan for aiding me with the experimental parts of this work. He has been a valuable friend and a trusted colleague for me. I would also like to thank Barbara Currie for all her great efforts and insightful guidance on the microbiology parts of my thesis.

I would also like to thank my colleagues, Lucas Karperien and Brent Godau, from the Laboratory for Innovations in Microengineering for their great help in reading and making constructive comments on my thesis.

I take this opportunity to express my profound gratitude to my parents for their emotional and moral support throughout my years of study. I have always been provided with their continuous encouragement and undivided attention.

Dedication

To my mentor, *Ali Sina Rahimi*, whose insights opened a new chapter in my life.

Introduction

An epidermal wound can be defined as a break or disruption in the anatomical structure of the epidermis and dermis (Lazarus et al. 1994). Wounds can be categorized into acute and chronic, based on their healing process (Lazarus et al. 1994). Acute wounds are usually caused by mechanical, chemical, and burn injuries with a complete healing time of 3-8 weeks and minimal scarring. In contrast, chronic wounds are attributed to wound reoccurrence or extended healing time – prolonged more than 12 weeks. Among various factors, infection, diabetes, malignancies, wound size, and underlying physiological conditions can be noted as the most common causes of wound healing failure and occurrence of chronic wounds (Harding et al. 2002; Boateng et al. 2008).

Demographics regarding wound-related diseases reveal the significance of research on wound treatment techniques, as 1% to 2% of the population in developed countries have been estimated to experience chronic wounds in their lifetime, posing a considerable burden on the health care system (Gottrup 2004). For instance, 6.5 million people have been reported to suffer from various sorts of chronic wounds in the United States alone, which entails an annual expenditure of $25 billion on wound-related medications (Järbrink et al. 2016). Similar statistics in Canada show that health system annually spends $3.9 billion for wound treatment which is approximately 3% of its total healthcare expenditure (Canadian Home Care Association, http://www.cdnhomecare.ca).

Wound healing process follows a cascade of events – involving cellular and matrix components – and in the case of healing, it leads to wound closure by the formation of new tissue. Despite the continuous nature of this process, it has been divided into

multiple overlapping phases, including hemostasis, inflammation, migration, proliferation, and maturation. During the first stage, bleeding is followed by hemostasis, in which clotting factors initiate the coagulation of the exudate. In this stage, the activation of fibrinogen by thrombin leads to the formation of a fibrin network and causes bleeding to stop by entrapping red blood cells and platelets (Schultz 1999; Temenoff & Mikos 2008). During the inflammatory stage, vasodilation – due to the presence of histamine and serotonin – facilitates the entrance of phagocytes to the wound site to engulf the necrotic tissue. In the next stage, epithelial cells – mostly keratinocytes – and fibroblasts migrate to the injured area to repair the damaged tissue and fill in the gap which is created by the wound (Schultz 1999). This process is mostly regulated by platelet-derived growth factors (Jones & Cross 2004). In the proliferative stage, the formation of the granulation tissue – a highly vascularized tissue composed of inflammatory cells and fibroblasts in a matrix of collagen, fibronectin, glycosaminoglycans, and proteoglycans – takes place 3-5 days post injury. Epithelialization, fibroplasia, angiogenesis, and wound contraction can be noted as other events in the proliferative phase, occurring up to 2 weeks after injury. During this phase, fibroblasts contribute to the further epithelial thickening by synthesizing collagen. Maturation or remodeling phase is the last stage in the wound healing process in which the formation of cellular connective tissue and epithelial layer develops the final scar tissue (Schultz 1999; Boateng et al. 2008).

Generally, medical care following an epidermal injury includes the removal of foreign materials, wound debridement (removal of necrotic tissue), drug therapy (e.g. prescription of antibiotics), and administration of a proper wound dressing. Moreover,

diagnosis of contributing diseases such as diabetes and anaemia plays an important role in taking a proper measure toward wound healing (Boateng et al. 2008). Various local and systemic factors have detrimental impacts on the wound healing process. Local factors include infection, inadequate blood supply, increased skin tension, wound dehiscence, the occurrence of foreign body reaction, local tissue mobility (e.g. around the joints), and hematoma. Moreover, several systemic factors such as physiological age, diabetes, obesity, malnutrition, and systemic malignancies can also deteriorate the epidermal injury into further medical complications (Nawaz & Bentley 2011).

Among the aforementioned contributing factors, infection accounts for a significant mortality, comprising about 75% of all deaths in burn patients (Church et al. 2006). Skin is a part of the innate immune system by functioning as a physical barrier to pathogens. In the case of epidermal wounds, namely burn wounds, disruption of this barrier may lead to a higher susceptibility to infection (Church et al. 2006). Wound infection is caused by the presence of microorganisms – commonly bacterial or fungal colonization – at the wound site. Common pathogenic bacteria in epidermal wounds include *Pseudomonas aeruginosa*, *Staphylococcus aureus*, *Staphylococcus pyogenes*, *Staphylococcus epidermidis*, and *Escherichia coli* (Boateng et al. 2013; Boateng & Catanzano 2015). Generally, wound infection results in a significantly reduced healing rate, increased treatment cost, and a higher mortality rate (Shupp et al. 2010).

This thesis has focused on the development of a multifunctional hydrogel-based wound dressing with the capability of detecting wound bacterial infection – based on the acidity of the wound environment – and delivering antibiotic to the wound site. After an overview of recent advancements on wound dressings, two 3-dimensional (3D)

bioprinting techniques will be discussed by which several components of the developed dressing have been fabricated. Finally, the aforementioned wound dressing will be introduced and its main characteristics will be discussed.

Chapter One: Advanced Wound Dressings

A wound dressing is a sterile pad or compress that covers the entire wound area to control bleeding, protect the wound from contamination, and minimize the risk of infection (Hospital Corpsman 2003). The main characteristics of a wound dressing are the ability to absorb blood and expedite the coagulation process (in the case of bleeding), controlling the wound moisture and removing excess exudate, biocompatibility and being non-allergic, permeability to gas exchange, impermeability to bacteria, ability to prevent further trauma, conformability, low cost, and having a reasonably long shelf life (Jones et al. 2006).

Traditional wound dressings – such as wool, cotton, gauzes, and natural and synthetic bandages – contribute passively to the wound healing process. These dressings, with different degree of absorbency, usually provide minimal evaporation control and results in wound dehydration. This dehydration usually causes the dressings to adhere to the wound and leads to patient discomfort when the dressing is removed for assessing the wound condition. Furthermore, the bacterial barrier created by most of these dressings is normally limited to the dry condition and might fail when the dressing is hydrated due to exposure to the wound exudate or external fluids. Despite their wide availability and low cost, traditional wound dressings have been replaced by advanced dressings particularly for treatment of burn and chronic wounds owing to the aforementioned issues. (Boateng et al. 2008).

Advanced wound dressings have been developed to address several challenges regarding their previous generations including but not limited to the provision of a more

effective microorganism barrier, antimicrobial delivery to the wound, and better control over the wound moisture content (Boateng & Catanzano 2015). Integration of *in situ* wound monitoring devices into wound dressings can also be noted as a significant progress toward the development of advanced wound dressings (Dargaville et al. 2013). To date, various sensing platforms have been developed and in some cases integrated with wound dressings to monitor different parameters including bacterial infection, change in biochemical composition, the level of moisture, and temperature at the wound site (Dargaville et al. 2013). Wound dehydration can be prevented by the use of materials with low water vapor transmission rate (WVTR) or hydrogels in wound dressings. Hydrogels are composed of a network of hydrophilic polymers with a high content of water by which they can provide a high biocompatibility (Peppas et al. 2006). The use of hydrogels, such as alginate and chitosan, in recently developed wound dressings have enhanced their water vapor transmission properties to provide a moist environment and facilitate the wound healing (Boateng et al. 2008).

The main purpose of this chapter is to review the recent breakthroughs in the development of advanced wound dressings with antimicrobial and infection tracking capabilities. After a brief overview of drug delivery in advanced wound dressings, the use of antimicrobial agents to inhibit infection will be explored. Antibiotics will be categorized based on their mechanism of action and several examples of each type will be provided. Subsequent sections explain traditional culture-based techniques for detecting bacterial infections and compare them with recent wound monitoring methods based on bacterial biochemistry and wound acidity. Finally, the role of the wound pH in determining its healing condition will be followed by discussing several pH sensors with

the capability of incorporation into wound dressings. It should be noted that development of cellular and acellular skin substitutes as another breakthrough in the treatment of epidermal wounds is not within the scope of this chapter, however, the use of 3D bioprinting for the generation of these engineered tissues will be discussed in the next chapter.

1-1- Wound dressings and drug delivery

In addition to their primary functions, wound dressings can accommodate the delivery of bioactive molecules to the wound site such as debriding agents to remove necrotic tissue, antimicrobial agents to inhibit microorganism growth, and growth factors to promote tissue regeneration (Boateng & Catanzano 2015). *In situ* drug-delivery – which can be implemented by the incorporation of polymeric substrates – provides a high drug dosage at the wound site while avoiding side effects resulting from systemic drug administration (Langer 1980). Furthermore, the sustained delivery of biomolecules with relatively short *in-vivo* half-lives – such as growth factors – can be facilitated by the aforementioned polymeric systems (Langer 1980). In polymeric drug delivery systems, drug release kinetics can be tuned by altering the effective parameters of polymeric substrate on the diffusion of encapsulated molecule toward its target. These parameters include substrate porosity, degree of swelling, and degradation rate (Slaughter et al. 2009).

Polymeric wound dressings have acquired special attention during recent years owing to their capability to incorporate the delivery of pharmacological agents into other primary functions of the dressings (Boateng & Catanzano 2015). Antimicrobial-loaded

dressings, in addition to functioning as a microorganism barrier, can actively eradicate bacteria or fungi present in infected wounds. In this regard, various components with antimicrobial activity – such as antibiotics, silver (e.g. in the form of nanoparticles), bacteriolytic enzymes, antimicrobial peptides, and poly(hexamethylene) biguanide hydrochloride (PHMB) – have been employed either in commercial dressings or scientific literature (Boateng & Catanzano 2015). This section explores the application of antibiotics and silver – two components with extensive use – in impregnated wound dressings.

1-1-1- Antibiotics in wound dressings

Antibiotics eradicate bacteria or inhibit their growth by various mechanisms based on preventing the development of components or blocking biological activities by which bacteria differ from human cells. These mechanisms include blocking bacterial cell wall development, degenerating or binding to the bacterial ribosome and therefore disrupting their protein synthesis, and impeding DNA replication (Reynolds 1989; Chopra & Roberts 2001; Cozzarelli 1977).

Despite limited clinical practices regarding antibiotic-loaded wound dressings, they have extensively been studied in the scientific literature (Boateng & Catanzano 2015). The use of antibiotics with the ability to inhibit protein synthesis (e.g. gentamicin, minocycline, and streptomycin) or prevent cell division (e.g ciprofloxacin) leads to a broad-spectrum effectiveness since these mechanisms target both gram-negative and gram-positive bacteria. Table1-1 summarizes several studies regarding the use of antibiotics in wound dressings based on their type and the employed biomaterials.

Mechanism of action on bacteria	Antibiotic	Wound dressing materials	Reference
Binding to bacterial ribosome	Gentamicin	Polyvinyl alcohol (PVA)-dextran hydrogel	(Hwang et al. 2010)
		Chitosan-gelatin composite film	(Bindu et al. 2011)
	Minocycline	Chitosan films	(Aoyagi et al. 2007)
		PVA- chitosan hydrogel	(Sung et al. 2010)
	Streptomycin	Polyox® carrageenan composite films	(Boateng et al. 2013)
		Polyox composite film	(Pawar et al. 2013)
Inhibiting DNA replication	Ciprofloxacin	Alginate-chitosan sponge	(Öztürk et al. 2006)
		PVA-poly(vinyl acetate) electrospun mats	(Jannesari et al. 2011)
		Dextran-polyurethane electrospun mats	(Unnithan et al. 2012)
Inhibiting bacterial cell-wall formation	Vancomycin	Chitosan sponge	(Stinner et al. 2010)
		Electrospun poly(lactic-co-glycolic acid) /collagen Nanofibrous membrane	(Chen et al. 2012)

Table 1-1- Antimicrobial-loaded wound dressings with different types of antibiotics.

In a notable study, Boateng *et al.* developed transparent films composed of polyethylene oxide and carrageenan and loaded them with streptomycin and diclofenac to be used as wound dressing (Boateng et al. 2013). Due to the anti-inflammatory properties of diclofenac, its combination with streptomycin – with antibacterial activity – was proposed to target the inflammatory phase and inhibit the infection during the wound healing process. They characterized the mechanical, swelling, and mucoadhesive

properties of the dressing, by which favorable absorbance characteristics and acceptable tensile strength were reported. Fabricated dressings showed an enhanced zone of inhibition against *Staphylococcus aureus*, *Pseudomonas aeruginosa*, and *Escherichia coli* compared to the condition with direct exposure to the antibiotic.

In another study, Aoyagi *et al.* used powder minocycline and chitosan films to fabricate a wound dressing with antimicrobial activity (Aoyagi et al. 2007). Figure 1-1 shows the components of this dressing that were supported by Tegaderm® – a commercial polyurethane film – as a backing to form a compound dressing for treatment of burn wounds. In this work, dressings were fabricated with chitosan with different deacetylation degree from 67% to 96% and two different amounts of antibiotics – 2 mg and 10 mg. They performed *in vitro* and *in vivo* drug release studies in which loaded antibiotic content was released within less than 12 hours. They also assessed the functionality of the dressing by *in vivo* tests on rats with severe burn wounds and reported a considerable pus reduction at the wound site by incorporating 2 mg of minocycline. In the *in vivo* test, the developed wound dressing demonstrated considerable advantages in terms of wound-dressing contact, the absorption of the exudate, and the elimination of the pus over a few commercial wound dressings including gauze, Beschitin™ W (Unichika Ltd., Japan), and Geben cream (Tokyo Tanabe Pharmaceutical Co. Ltd., Japan).

In another work, Stinner *et al.* reported a considerable impact on bacteria reduction in created musculoskeletal wounds on goats by incorporation of amikacin and vancomycin (Stinner et al. 2010). They employed chitosan sponges to encapsulate amikacin for wounds contaminated with *P. aeruginosa* and vancomycin for wounds infected by *S. aureus*. Chitosan sponges were tuned to degrade over 48 to 72 hours and led to a

significant quantity reduction in both types of bacteria 6 hours following the treatment. They used 32.5 mg of antibiotic for each type of contamination and showed that serum antibiotic level remained less than 15% of this level in systemic treatment.

As discussed, antibiotics can be effectively incorporated into wound dressings to impede certain sorts of infection. However, the emergence of antibiotic-resistant strains of bacteria and inability to inhibit non-bacterial infection have posed limitations on their application in wound dressings. In mentioned cases, silver can be noted as an alternative antimicrobial agent with a wider range of effectiveness.

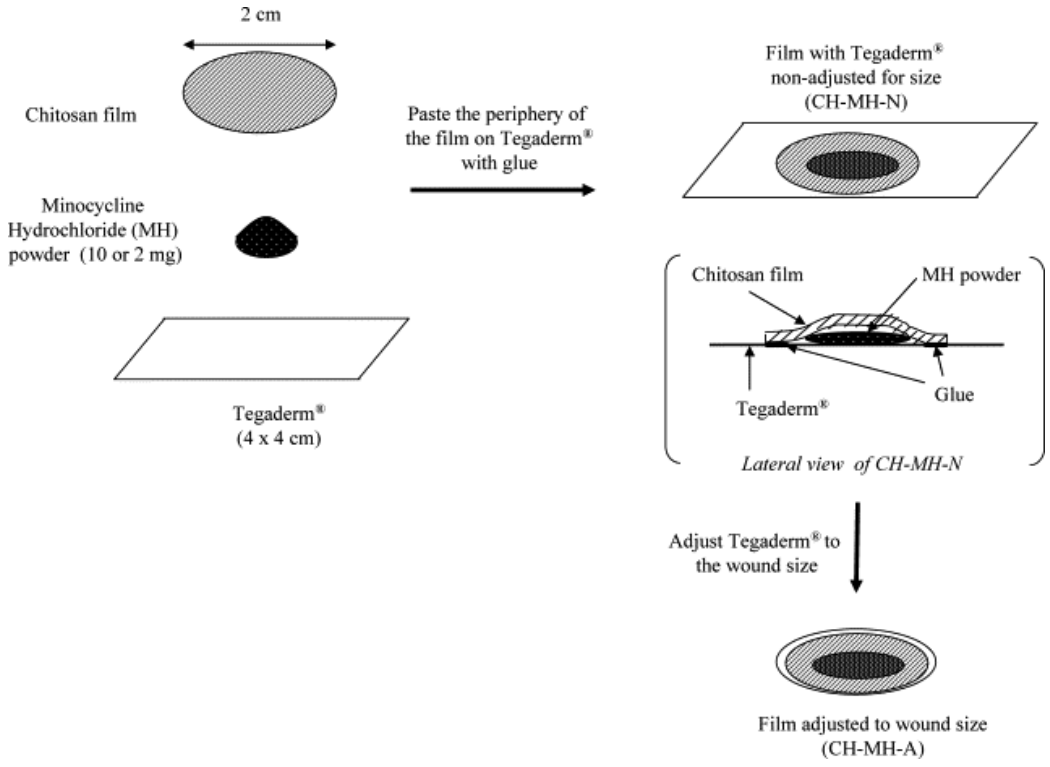

Figure 1-1- Fabrication of wound dressings composed of chitosan, minocycline, and Tegaderm®. Reproduce with permission (Aoyagi et al. 2007).

1-1-2- Silver-loaded wound dressing

Silver has been shown to have an antimicrobial impact on a relatively wide pathogen spectrum by various mechanisms (Boateng & Catanzano 2015). Silver can affect both

gram-negative and gram-positive bacteria. It has been widely used in commercial wound dressings in different forms including elemental silver, ionic silver, silver oxide, silver sulfate, and silver chloride among many others (Pant et al. 2012; Boateng & Catanzano 2015). Inhibition of bacterial growth, nonspecific to bacteria type, and affecting nonbacterial infection sources such as fungi are the advantages of using silver over antibiotics in wound dressings (Gemmell et al. 2006) However, the cytotoxic effect of silver ions on human cells is one of the drawbacks of silver-loaded wound dressings.

Different mechanisms have been proposed for the bactericidal effect of silver ions. They disrupt transmembrane energy generation and electrolyte transport by deactivating involving thiol-containing enzymes through making insoluble compounds with their thiol groups in the cell wall (Williams et al. 1986). Silver ions can also inhibit the respiratory chain in bacteria (Jansen et al. 1994). As another proposed mechanism, silver ions can cause DNA denaturation by opening hydrogen bonds between adjacent purines and pyrimidines (Klueh et al. 2000).

In a notable study, Klueh *et al.* employed silver coating to develop a bactericidal fabric (Klueh et al. 2000). In this study, poly(ethylene terephthalate) fabric was coated with metallic silver by an ion-beam assisted deposition system to release silver ions (Ag^{2+}) at the wound site. Their *in-vitro* test showed a considerable reduction in cell growth rate from 0.78 h^{-1} to 0.15 h^{-1} in *Staphylococcus epidermidis*.

Silver nanoparticles (AgNPs) have also achieved a wide popularity due to their high-surface-area-to-volume ratio; this characteristic affords high diffusive flux of silver ions by using relatively low concentrations of AgNPs (Madhumathi et al. 2010). For instance, Pant et al. demonstrated the antibacterial activity of hybrid nanofibers made of nylon-6

nanofibers and coated with AgNPs (Pant et al. 2012). In this study, they employed electrospinning to fabricate nanofibers and solvent reduction to *in situ* form and assemble AgNPs on electrospun fibers. As shown in Figure 1-2, developed nanofibers represented antibacterial impact on *E. coli* and *S. aureus* and proposed for use in wound dressings and water filters.

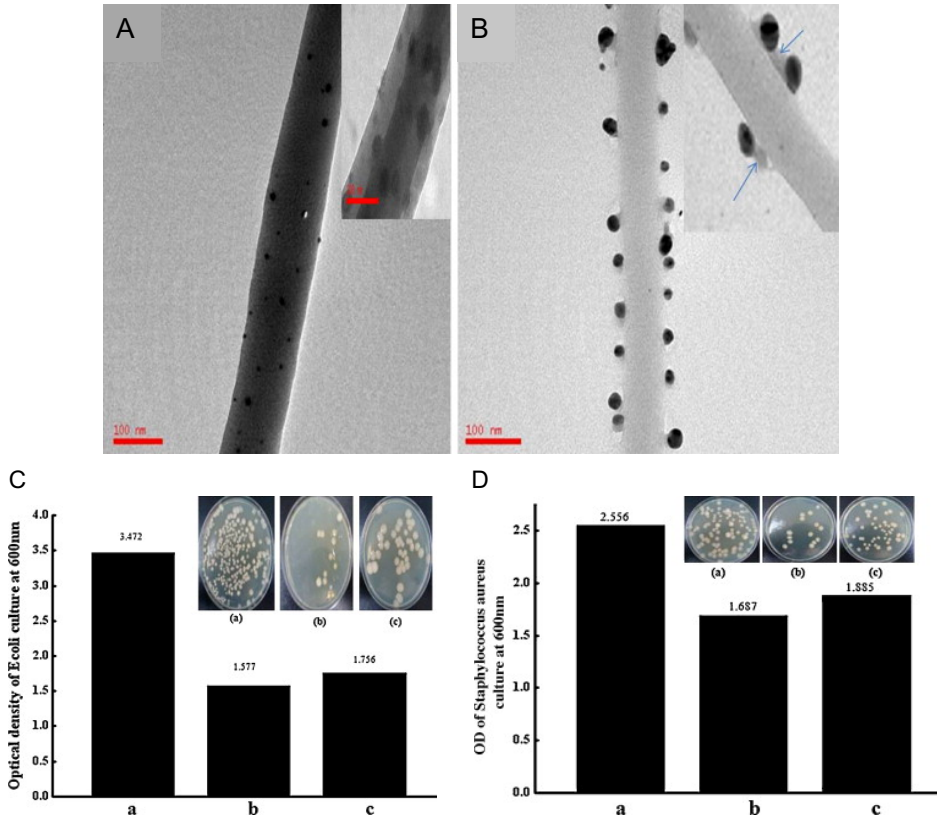

Figure 1-2- A, B) Fabricated nylon-6 nanofibers with two different loading process (m1, left and m2, right) for AgNPs. B, C) Antibacterial effect on *E. coli* and *S. aureus* with (a) control nanofibers, (b) m1, and (c) m2 conditions. Reproduced with permission (Pant et al. 2012).

While targeting a wide range of bacterial and fungal infections, silver has been reported to have cytotoxic effects on fibroblasts and macrophages, affecting their metabolic activity, damaging their membrane, and causing apoptosis by oxidative stress (Cheng et al. 2013; Park et al. 2011). As fibroblast and macrophages are the key components during several wound healing stages, this detrimental impact can negatively influence an

effective wound healing. In this term, antibiotics are relatively nontoxic, while affecting a narrower range of infections (Lipsky & Hoey 2009). It has been shown that silver nanoparticles have reduced cytotoxicity to fibroblast and macrophages when they are within certain size ranges (Park et al. 2011). This can partially address the toxicity concern while requiring a more complicated fabrication process. Similar to antibiotics, silver resistance can be developed by different types of bacteria such as *Pseudomonas* and *Enterobacteriaceae* families, leading to ineffectiveness and another challenge regarding the use of silver in wound dressings (Silver et al. 2003); however, this failure is less frequent with silver compared to antibiotics (Lipsky & Hoey 2009). All mentioned factors concerning the use of silver and antibiotic in wound dressings represent the need for a careful consideration for administering a proper antimicrobial agent according to the type of infection.

1-2- Methods for detecting infection

Various methods based on analysis of wound specimen or *in situ* wound monitoring have been developed for detecting infection in epidermal wounds. Gram staining, surface swab culture, quantitative tissue culture, and histological analysis can be noted as common traditional procedures to detect pathogens present in wounds based on the analysis of wound samples (Church et al. 2006). Among the mentioned approaches, culture-based techniques allow for the identification of pathogens and antimicrobial susceptibility analysis to take a proper measure against the microorganisms present in the wound. In contrast to traditional methods, recent techniques have targeted different

indicators for detecting infection such as the biochemical activity of bacteria, odour, the acidity of the wound exudate, and wound temperature (Dargaville et al. 2013).

Among the traditional methods, gram staining technique aims to distinguish bacteria type according to their cell wall structure, gram-positive and gram-negative. This method can be implemented on collected wound specimens to facilitate wound infection diagnosis. Surface swab culture can detect and quantify the number of viable bacteria, present in open wounds (Levine et al. 1976). This method eliminates the need for surgical manipulation of the wound, however, it fails to detect non-superficial infections. Quantitative biopsy culture is the most accurate method for wound infection surveillance (Church et al. 2006). In this method, the presence of bacteria with more than 10^5 cfu/gr of the tissue specimen indicates infection according to the histological studies (Loebl et al. 1974). In histological analysis – as the last analytical method performed on biopsy specimens – wound infection is diagnosed when microorganisms' invasion is observed in the subjacent tissue (Mitchell et al. 1989).

All aforementioned analytical methods require specimen collection. This requirement entails periodic replacement of the wound dressing, exposure to the environment which increases the chance of infection, and inflicting pain to the patient. In this case, various reasons including the possibility of a non-infectious diagnosis after all mentioned experimental efforts and non-reproducibility potential based on the region of sample collection have necessitated *in situ* wound monitoring for early detection of infection (Church et al. 2006). This form of wound surveillance has been implemented through wound dressings with the capability of real-time wound monitoring (Dargaville et al.

2013; McLister et al. 2014). In the next sections, several infection indicators based on bacterial biochemistry and wound pH will be discussed.

1-2-1- Use of bacterial biochemistry for detecting infection

Methods concerning bacterial biochemistry focus on a broad range of diagnostic targets such as bacterial by-products. Substances such as pyocyanin, uric acid, neutrophil elastase, phospholipase A_2, and α-hemolysin among many others can be noted as the biochemical indicator of infection (Dargaville et al. 2013). Some of these markers have been employed in an integrated form with wound dressings and some have been developed for use in point-of-care assessments.

For instance, pyocyanin – a phenazine dye secreted by gram-negative *P. aeruginosa* – was considered by Sharp *et al.* as an infection indicator (Sharp et al. 2010). In this study, they developed a pyocyanin sensor composed of a carbon fiber tow to detect oxidation and reduction of phenazine based on square wave voltammetry (Figure 1-3). They were able to measure the concentration of pyocyanin within the range of 1-100 μM and subsequently quantified *P. aeruginosa* in broth culture. The developed sensor was proposed for use in point-of-care testing devices.

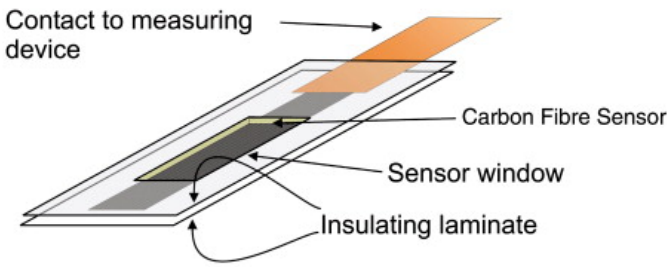

Figure 1-3- Carbon fiber sensor assembly for detection of pyocyanin. Reproduced with permission (Sharp et al. 2010).

The same group developed a carbon fiber sensor for electrochemical sensing of uric acid based on its oxidation (Sharp et al. 2008). Uric acid is metabolized by some species such as *S. aureus* and *P. aeruginosa*, in which case, a decrease in uric acid concentration in wound fluid can be a sign of bacterial infection. They thermally sandwiched carbon fibers between polyester laminates and employed similar square wave voltammetry at 0.23 V to quantify uric acid concentration. Figure 1-4 shows their proposed method for using the developed sensor directly at the wound site. They reported an accurate measurement of uric acid concentration in blood and blister fluid, however, their method showed a drawback of electrode failure over time, which was partially addressed by using a cellulose acetate barrier.

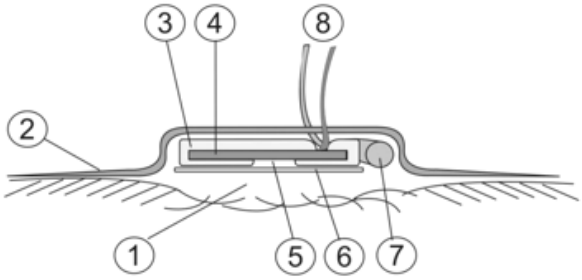

Figure 1-4- Schematic demonstration of a wound dressing equipped with a carbon fiber sensor to detect uric acid. (1) wound, (2) backing bandage, (3) laminate, (4) carbon fiber sensor, (5) sensor window, (6) cellulose acetate barrier, (7) Ag/AgCl counter electrode (8) ports to the measurement device. Reproduced with permission (Sharp et al. 2008).

1-2-2- pH as an indicator of infection

The acidity of skin is an indicator of its health without any gender-specific difference (Zlotogorski 1987). The pH of the healthy skin is within the range of 4-6, and in the case of injury, it becomes in equilibrium with internal body fluid (pH 7.4). The normal acidic milieu is due to the presence of fatty acids, amino acids, and some other substances

produced by keratinocytes (Schneider et al. 2007). This acidic environment also functions as a part of the innate immune system since most of the human-pathogenic microorganisms cannot grow in environments with pH value less than 6 (O'Meara et al. 2000). The acidity of a wound varies in different healing stages, and pH of an acute wound differs from a chronic wound. As shown in Figure 1-5 A, in an acute wound, pH decreases toward acidic condition during the inflammation stage and increases to basic condition during granulation stage. Finally, pH reaches to the normal value after the reepithelization stage. In contrast, pH of a chronic wound follows a more complicated pathway and alters mostly in a slightly basic condition, as indicated in Figure 1-5 B (Schneider et al. 2007).

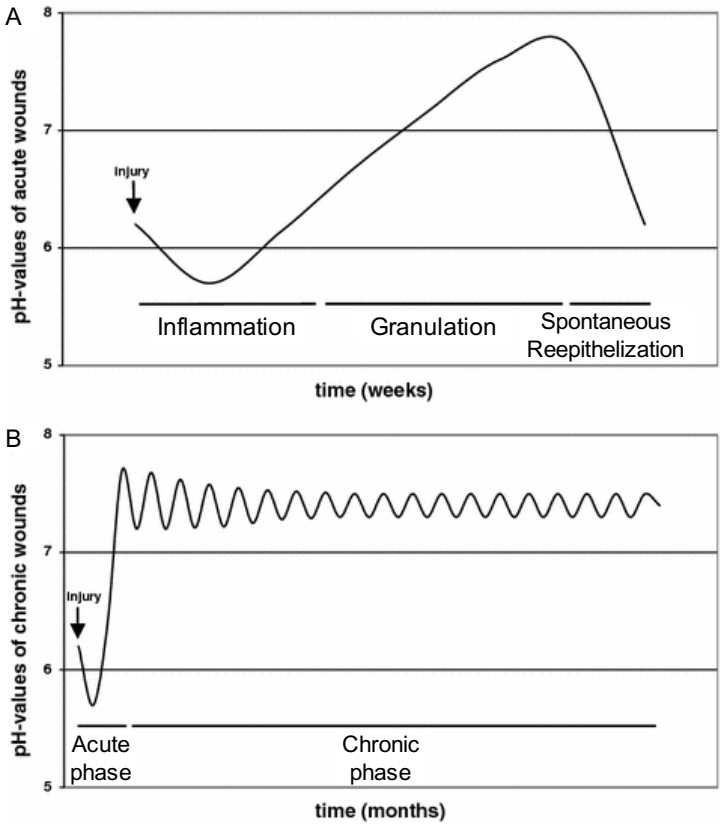

Figure 1-5- (A) pH change in acute wounds. (B) pH change in chronic wounds. Reproduced by permission (Schneider et al. 2007).

In the case of an infection, microbial metabolism alters the pH of the wound (Shi et al. 2011; Srinivasan & Mahadevan 2010). For instance, in a study on two strains of bacteria, Srinivasan *et al.* showed that *E. coli* and *Geobacter sulfurreducens* have different proton consumption/secretion behavior in various culture media in aerobic and anaerobic conditions, leading to pH change in their environment to either acidic or basic state. A similar outcome has resulted from a study on other families of bacteria including *Pseudomonas*, *Staphylococci*, and *Fusobacterium* (Shi et al. 2011). Accordingly, this pH change, as a result of bacterial growth, can be used as an indicator for detecting bacterial infection. Various techniques have been employed for measuring pH in wound dressings, including colourimetry, use of hydrogels with pH-dependent swelling behavior, and electrochemical sensing methods (Dargaville et al. 2013).

The use of halochromic materials, which change colour with pH variation, is one of the simplest and most common methods to track pH variation (Dargaville et al. 2013). These materials absorb different wavelengths of visible light based on the acidity of their environment and produce different colours. Several natural materials such as cabbage juice (Chigurupati et al. 2002) has been recognized as halochromic among various synthetic pH-responsive dyes with the capability of tracking pH in a certain range. In this method, correlation of colour change and pH facilitates the used of colourimetry and image processing for determining the pH value. In a recent study, Tamayol *et al.* utilized Brilliant Yellow – a commercially available pH-responsive dye – to fabricate pH-responsive hydrogel fibers with the application for detecting infection at the wound site (Tamayol et al. 2016). They immobilized the halochromic dye with onion exchange resin microbeads which were embedded into alginate hydrogel. Fabricated fibers enabled the

pH measurement ranging from 5.5-9 and were capable of being incorporated into commercial wound dressings.

As another approach to the use of pH sensors in wound dressings, a pH-responsive hydrogel was employed by Sridhar *et al.* with a pH-dependent swelling ratio (Sridhar & Takahata 2009). The hydrogel was sandwiched by a folded flex-circuit, including an inductive transducer to detect pH based on the displacement of folded plates as a function of hydrogel swelling. A wireless frequency measurement system was integrated with the sensor to monitor the resonant frequency of the device and track the pH value. They assessed the functionality of the developed sensor by measuring the acidity of buffers with variable pH, ranging from 2 to 7.

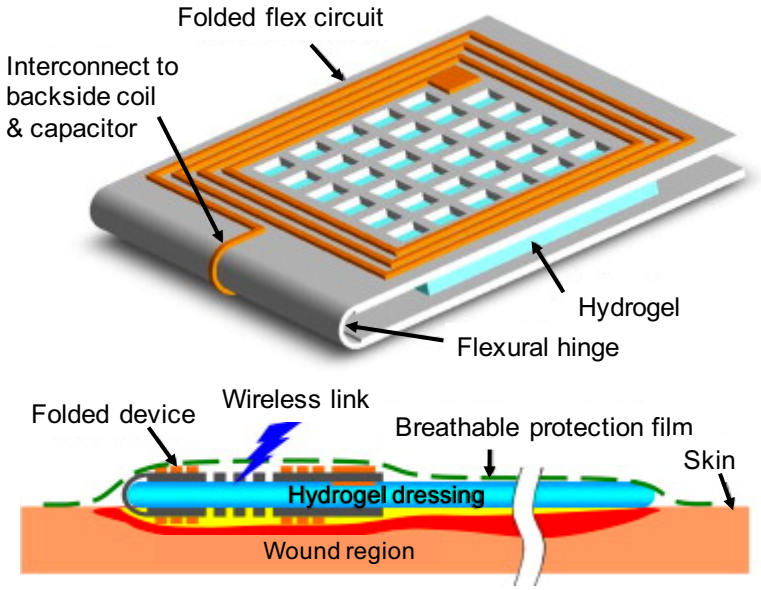

Figure 1-6- Schematic of the fabricated pH sensor composed of a pH-sensitive hydrogel and a flex-circuit (up). The capability of the sensor to be integrated with a commercial wound dressing. Reproduced with permission (Sridhar & Takahata 2009).

Figure 1-6 demonstrates the schematic of the developed pH sensor combined with a commercial wound dressing, 2nd Skin™ sandwiched inside the folded flex circuit, representing the potential of this combined system for wound healing application. Despite

the accuracy of this system for *in-vitro* pH measurement, in practical condition, change in water content of the hydrogel due to evaporation or absorption might affect the hydrogel thickness and therefore interferes with the pH reading.

In another study, Mostafalu *et al*. fabricated a thread-based diagnostic device for measurement of pH, temperature, glucose, and strain in biological tissues (Mostafalu et al. 2016). The developed sensing platform could be sutured into the target tissue or placed on a substrate such as epidermis. They coated cotton threads with various conductive inks containing silver, silver chloride, carbon, carbon nanotubes (CNTs), and polyaniline (PANI). In this system, CNT-coated threads served as resistive temperature sensors for monitoring tissue temperature – as an indicator of inflammation and bacterial infection. For pH measurement, they manipulated the wicking property of the thread into the generation of a microfluidic splitter by patterning threads on a hydrophobic woven fabric. In this microfluidic platform, the conductivity of the PANI-coated threads depended on the protonation and deprotonation condition of the coating, creating a pH-dependent response based on the acidity of the absorbed fluid. The developed pH sensors enabled the acidity measurement in buffer solutions with different pH values, ranging from 3 to 8. They also conducted *in-vivo* assays on rat models to demonstrate the capability of this microfluidic-based sensor to measure the subcutaneous pH value.

1-3- Conclusion

Infection in epidermal wounds has been a growing concern due to its dire consequences including subsequent medical complications, delayed wound healing, and increased cost and mortality. Many recent approaches to wound treatment have been

focused on the incorporation of either wound monitoring or drug delivery into wound dressings. However, combining monitoring and drug delivery systems into an integrated platform and creating an optimal condition to track and facilitate the wound healing process has been a challenge.

Drug delivery to the wound has been implemented using various antimicrobial agents, namely, silver and antibiotics. Incorporating silver into wound dressings can facilitate the inhibition of a wide range of infections caused by bacterial and nonbacterial sources along with antibiotic-resistant strains of bacteria. Silver in various forms has been extensively used in commercial wound dressings. Silver nanoparticles have particularly received a great attention due to their high surface-area-to-volume-ratio, enabling a high rate of silver ion diffusion to the wound. In spite of mentioned advantages, cytotoxicity of silver and its negative impact on fibroblasts and macrophages – as essential components of wound healing process – have posed limitations to the use of this antimicrobial agent. On the other hand, antibiotics have been shown to be relatively nontoxic to fibroblasts and macrophages compared to silver products, while targeting a more specific type of microorganisms. Bacterial growth can efficiently be inhibited by antibiotics among which broad-spectrum types can affect a wide range of bacteria – both gram-negative and gram-positive – by disrupting their protein synthesis or cell division process.

Various techniques have been developed to detect wound infection based on specimen collection or use of *in situ* sensing devices. Traditional approaches to detect infection mostly focus the culture of wound specimens, enabling the quantitative assessment of microorganisms present in the wound. While traditional methods can provide valuable information regarding the type of infection – necessary for antimicrobial susceptibility

analysis – *in situ* wound monitoring systems can accommodate infection tracking in a real-time manner. During recent years, there has been a great effort to incorporate infection sensors into wound dressings. These systems employ different indicators for infection, among which pH can accommodate tracking the wound condition with various techniques such as colourimetry. In this case, change in wound acidity can be interpreted as the possibility of microorganism colonization. *In situ* infection monitoring systems can determine the need for further culture-based analyses without inflicting unnecessary pain to the patient.

Chapter Two: 3D Printing – an Enabling Technology for the Fabrication of Wound Dressings

Three-D printing was first developed in the early 1980s and used for the construction of plastic parts (Hull 1986). 3D printing – synonymous with additive manufacturing – is the layer-by-layer deposition of materials to fabricate a 3D structure. Computer-aided design (CAD) and computer-aided manufacturing (CAM) are the key concepts in 3D printing, by which a 3D structure is modeled and transcribed to code to provide the controlled special movement accompanied with material deposition. 3D bioprinting was developed by combining the concept of 3D printing with cell biology and material science (Murphy & Atala 2014). Due to the ability to fabricate complex structure with desired spatial resolution and facilitate material versatility, 3D bioprinting has acquired many applications in the biomedical sector, namely tissue engineering (Murphy & Atala 2014; Kang et al. 2016; Pedde et al. 2017), developing medical devices (Zopf et al. 2013), and cancer research (Knowlton et al. 2015).

2-1- Application of 3D bioprinting in wound dressing and skin substitutes

Among various applications in biomedical engineering, 3D bioprinting has also received attention in the development of wound dressings (Rees et al. 2015; Murphy et al. 2013; Anon 1989). The capability of 3D bioprinting to control the porosity of fabricated constructs has been utilized for developing the potentials for delivery of antimicrobial components to the wound. As an example, Rees *et al.* have fabricated microextrusion-based 3D bioprinted films – composed of different types of nanocellulose – to be used as wound dressings (Rees et al. 2015). The developed dressings were tested on *P.*

aeruginosa and showed bacterial growth inhibition. In another study, Murphy *et al.* employed a pressure-driven inkjet system with the potential to 3D print a range of hydrogels directly to the wound site for treatment of deep dermal wounds (Murphy et al. 2013). The proposed system was able to integrate with a laser scanner to create a model of the wound geometry and control the hydrogel deposition system accordingly. In this study, hydrogel products, based on different sources including collagen, alginate, hyaluronic acid, chitosan, and polyethylene glycol, were employed. Based on *in-vitro* assays, they reported induced proliferation of keratinocytes which is essential to accelerate the healing rate.

Generation of skin substitutes can be noted as another application of 3D bioprinting for the treatment of chronic wounds. Suitable spatial resolution of this biofabrication strategy – particularly by laser-assisted material deposition – enables the precise positioning of multiple cell types with high cell viability (Murphy & Atala 2014). To illustrate this, in a previous study, Michael *et al*. utilized a laser-assisted 3D bioprinting system to fabricate cellularized skin substitutes (Michael et al. 2013). They have taken advantage of 3D bioprinting to deposit keratinocytes and fibroblasts on Matriderm® – an acellular dermal substitute. As shown in Figure 2-1, developed cellularized skin substitutes were implanted into nude mice with full-thickness skin wounds, using dorsal skinfold chambers. They reported a full integration of skin grafts with the surrounding tissue 11 days after the implantation. Laser-assisted 3D bioprinting was also employed by another group in Germany to develop multicellular skin grafts (Koch et al. 2012). In this work, keratinocyte- and fibroblast-laden collagen was printed layer-by-layer to form a 3D structure, demonstrating the capability of this biofabrication method to apply specific

micropatterning. They reported a promising functionality for their engineered tissue by observing the developed adherens junctions and suitable cell proliferation after 10 days of tissue culture.

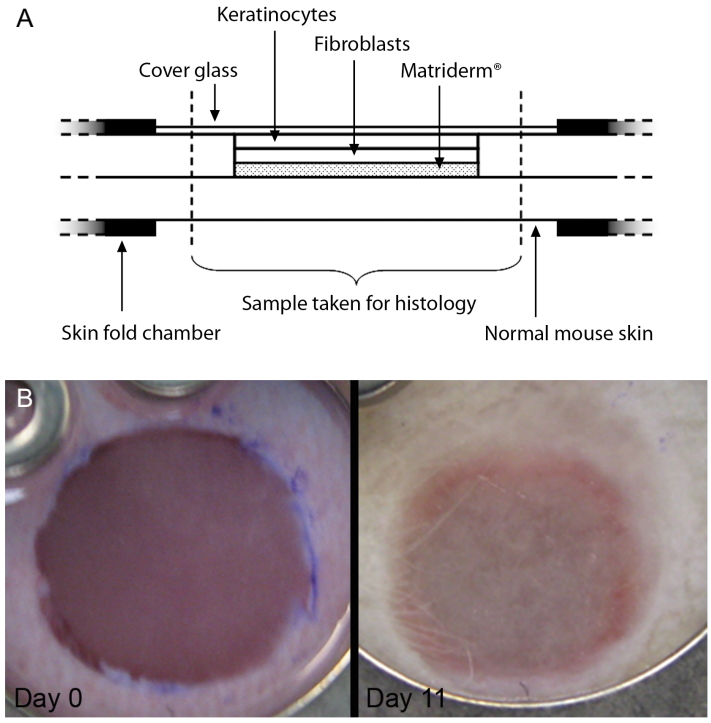

Figure 2-1- Schematic and *in vivo* demonstration of the engineered skin tissue fabricated by laser-assisted 3D bioprinting. A) The fabricated skin substitute was placed into the full-thickness skin wound using a dorsal skinfold chamber which was closed by a glass cover. B) Skin tissue after implantation (left) and on day 11 (right) in a mouse. Reproduced with permission (Michael et al. 2013).

This chapter represents the use of 3D bioprinting for the fabrication of porous constructs which were further used as pH sensors and drug releasing components in a developed wound dressing. As discussed in the next chapter, mentioned 3D printed constructs were embedded into a hydrogel patch to perform antibiotic delivery and infection monitoring at the wound site. Generation of porous constructs with desired diffusive properties accompanied with creating a platform to produce an array of 3D structures can be noted as the main rationale behind the use of 3D bioprinting in this

project. The main component of bioink in this 3D printing system was sodium alginate solution, deposited with microextrusion methods. As indicated in Figure 2-2, the fabrication system comprised of two syringe pumps (Harvard Apparatus) and a microextrusion system which were incorporated into a commercial 3D printer (Prusa i3).

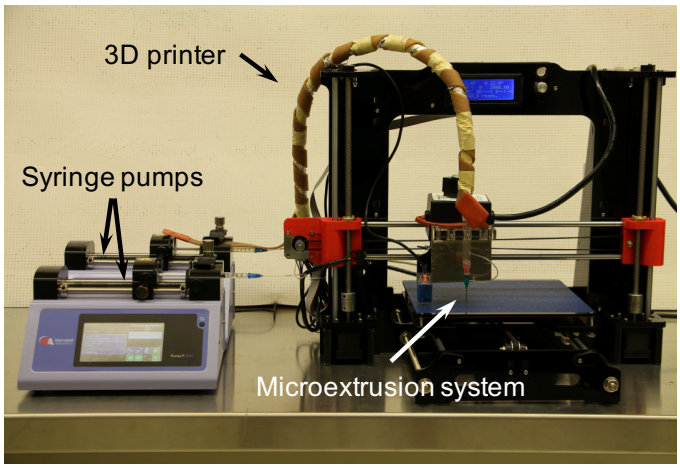

Figure 2-2- 3D bioprinter composed of two syringe pumps, a microextrusion system, and a commercial 3D printer.

2-2- Materials and methods

Two previously developed microextrusion methods (Luo et al. 2013; Barbetta et al. 2014) were adapted and characterized to afford deposition of our microparticle-laden bioink and create 3D constructs with desirable structural properties.

In the first method, a single 200-μl pipette tip (VWR International) was attached to a 3-ml plastic syringe (Terumo, Japan) and used for extruding sodium alginate solution with relatively high concentrations (typically 16% w/v). In this single-channel extrusion system, the high concentration of sodium alginate contributed to the formation of polymeric fibers. In this case, the high viscosity of the fluid maintained the morphology of the 3D-printed construct. Sodium alginate solution was extruded using a 3-ml syringe

connected to a syringe pump with flow rates ranging from 20 μl/min to 40 μl/min. printing speed varied between 1.5 mm/s and 5 mm/s. The printed structure was then crosslinked by soaking in calcium chloride solution (2% w/v).

In the second method, sodium alginate solution with concentrations ranging from 2% (w/v) to 6% (w/v) in distilled water was loaded into a 3-ml syringe, attached to a syringe pump. The polymer solution was supplied with flow rates ranging from 70 μl/min to 90 μl/min. Calcium chloride solution, as the crosslinking agent, with 6% (w/v) concentration was loaded into the same type of syringe and supplied by another syringe pump. Printing speed was ranged from 3 mm/s to 7 mm/s.

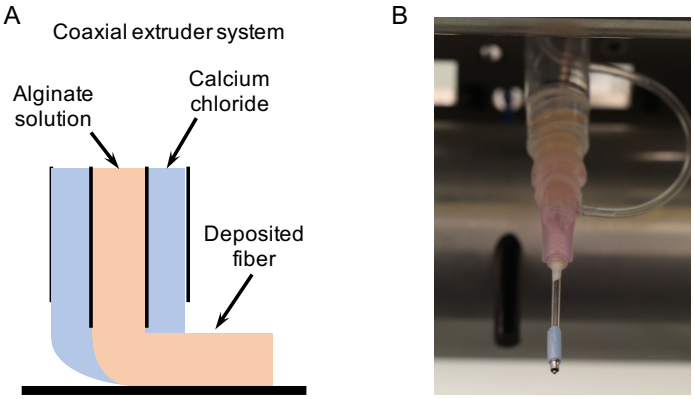

Figure 2-3- A) Schematic of the microfluidic system for ionic crosslinking of sodium alginate and formation of the hydrogel. B) Photographic image of the microfluidic system made of two coaxial hypodermic needles.

In this method, the microextrusion system comprised of a microfluidic device with coaxial core and sheath channels in which alginate and calcium chloride solutions were flowing, respectively. As shown in Figure 2-3, alginate hydrogel was ionically crosslinked at the tip of the extruder and deposited on the printer's bed.

For the fabrication of the coaxial microfluidic system, two hypodermic needles were attached to each other coaxially and the inner needle (20 gauge) was fixed and

maintained concentrically with the outer needle (15 gauge) by making small dimples on the sheath needle's sides. Then, sheath and core needles were connected to the calcium chloride and alginate syringes, respectively, by flexible tubings (VWR, Tygon Microbore, 0.020"×0.06").

2-3- Results and discussion

The capabilities of each 3D printing method were determined by performing this process with different printing specifications – printing speed and material deposition rate – and observing the characteristics of the fabricated hydrogels. While the single-channel extrusion method allowed for the generation of two-layer hydrogels, fabrication of multi-layer constructs was possible with the coaxial-extrusion system. This difference resulted from the simultaneous crosslinking of sodium alginate and material deposition in the coaxial-extruder which led to the formation of a stable fiber during the printing process. In contrast, printing more than two layers with the single-channel extruder led to the fusion of non-crosslinked polymer fibers.

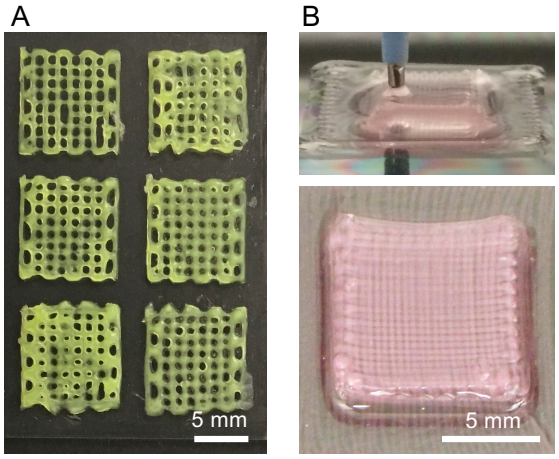

Figure 2-4- A) 3D bioprinted alginate hydrogels with single-channel extrusion method. Printing time for each hydrogel construct was 90 seconds. B) Photographic image of the 3D

printing process (top) and a 3D printed hydrogel (bottom) generated by the coaxial extrusion method. Printing time for each layer of hydrogel was 30 seconds.

The coaxial extrusion system accommodated a faster printing process with a typical printing speed of 6 mm/sec, while the high viscosity of bioink in the single-channel extrusion method led to the ideal printing speed of 2 mm/sec for fabrication of hydrogel fibers with uniform morphology. Hydrogel constructs fabricated by single-channel extrusion method possessed a better structural integrity due to the entire crosslinking of polymer structure after the printing process, and therefore, integration of printed fibers. Figure 2-4 demonstrates the fabricated hydrogel constructs and their printing time with both 3D printing methods.

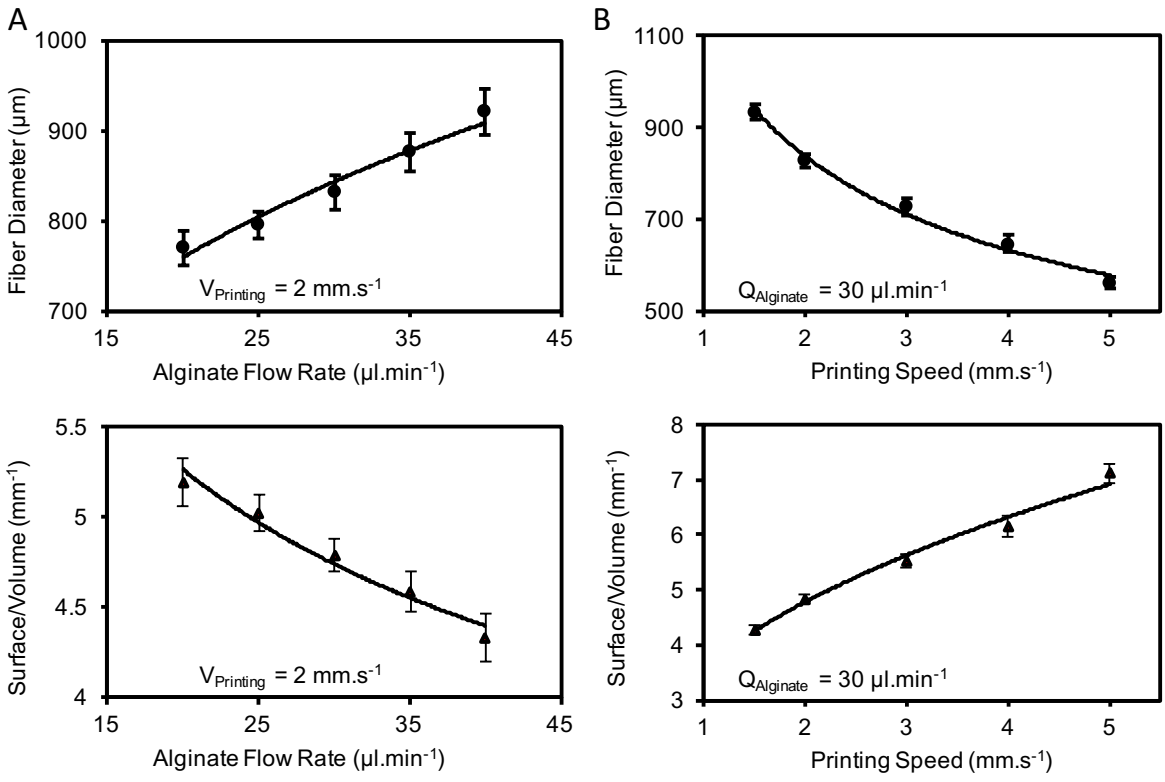

Figure 2-5- Variation of fiber diameter and surface-area-to-volume ratio based on the change in (A) alginate flow rate and (B) printing speed for single-channel extrusion method. Error bars are standard deviation (SD) (n=6).

Both microextrusion 3D printing methods enabled control over fiber diameter by adjusting either the printing speed or the polymer extrusion rate. In these cases, increase in printing speed led to a decrease in fiber diameter, while larger fibers were achieved by using higher flow rates for alginate. For the single-channel extrusion system, variation of flow rate from 20 μl/min to 40 μl/min led to a change in final fiber diameter from 770 μm to 920 μm. On the other hand, fiber diameter changed from 930 μm to 560 μm by increasing printing speed from 1.5 mm/sec to 5 mm/sec. The use of coaxial-extruder system afforded higher flow rates for the polymer solution due to a lower concentration of alginate and therefore lower viscosity. In this printing method, the flow rate of the polymer solution was altered from 70 μl/min to 110 μl/min and resulted in fabrication of fibers with a diameter ranging from 550 μm to 640 μm. Variation of printing speed in this system from 2 mm/sec to 7 mm/sec led to a change in fiber diameter from 600 μm to 530 μm. The surface-area-to-volume ratio, one of the important characteristics of the 3D construct, has a reverse relation to fiber diameter, as larger fiber diameter results in lower surface-area-to-volume ratio. Variation of fiber diameter and surface-area-to-volume ratio in different printing speed and alginate flow rates for single-channel and coaxial extrusion systems are indicated in Figure 2-5 and Figure 2-6, respectively.

The significance of the surface-area-to-volume ratio is due to its considerable impact on the diffusive behavior of 3D printed constructs. Since 3D printed structures were used as pH sensors or drug-releasing components, diffusion-based transport is the main mechanism of mass transport, determining the drug release kinetics and the sensors' response time. Generally higher surface-area-to-volume ratio results in higher diffusive

flux, and therefore, faster transport of drug and hydrogen ions through the hydrogel construct.

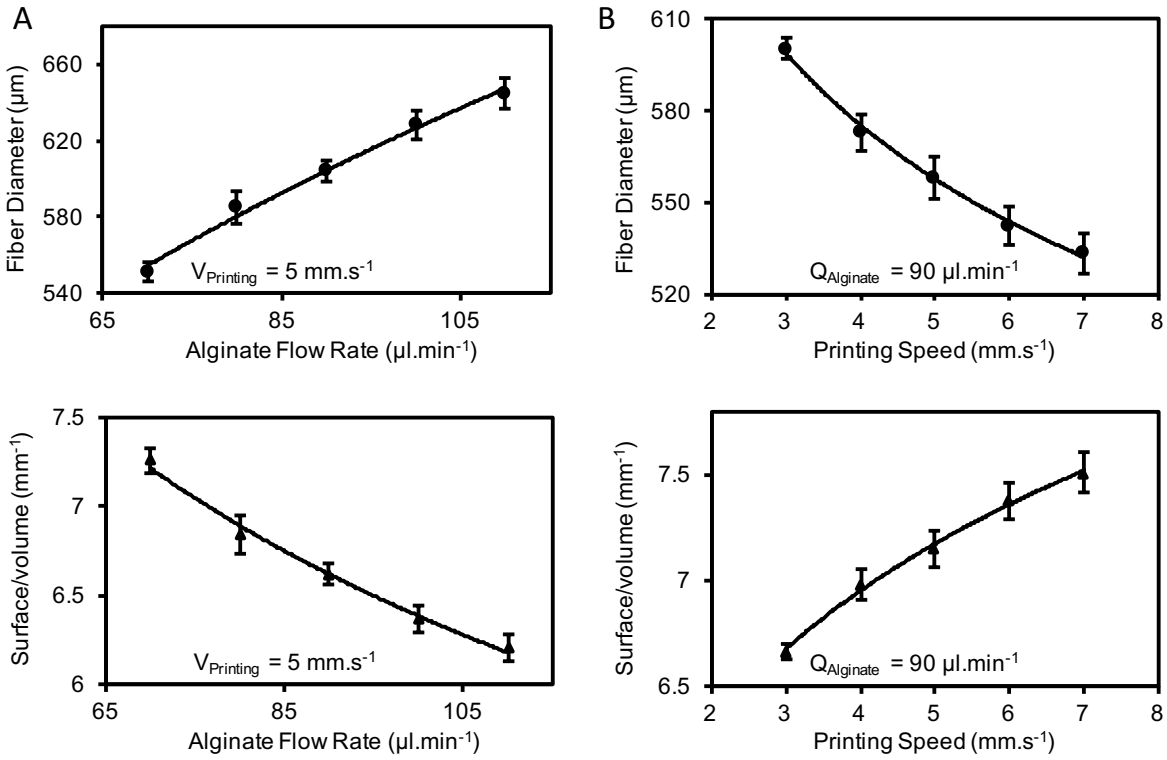

Figure 2-6- Variation of the fiber diameter and surface-area-to-volume ratio based on the change in (A) alginate flow rate and (B) printing speed for coaxial extrusion method. Error bars are SD (n=6).

Printability of both printing methods was assessed by conducting the printing process with different concentrations of alginate and a fixed condition of crosslinking agent. Alginate concentration varied from 2% (w/v) to 16% (w/v) for both printing conditions, and calcium chloride concentration was kept constant at 6% (w/v) for the coaxial microfluidic method. As demonstrated in Figure 2-7, the single-channel extrusion method enabled the printing process only with the highest concentration of alginate; however, with the coaxial microfluidic system, the formation of a 3D printed structure was feasible for a wider range of alginate concentrations, from 2% (w/v) to 6% (w/v).

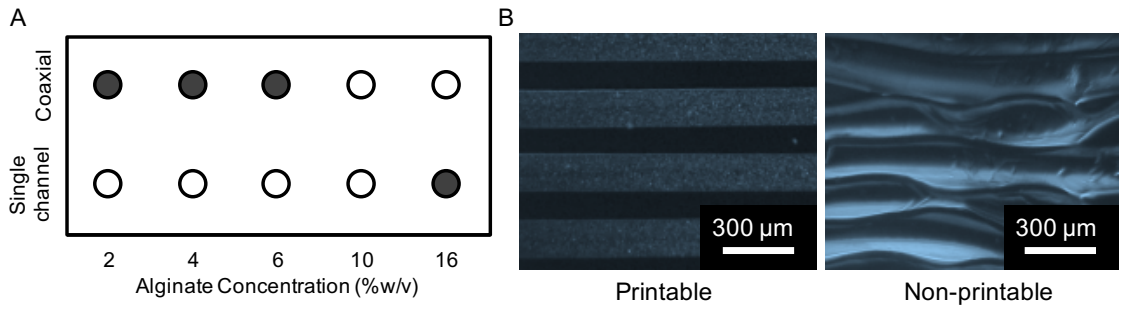

Figure 2-7- A) Printability of single-channel and coaxial extrusion methods for different concentration of alginate. Black circles show printable and white circles show non-printable conditions. B) Printable and non-printable samples are shown by bright field microscopy typically for coaxial/alginate 4% (w/v) and coaxial/alginate 10% (w/v) conditions, respectively.

2-4- Conclusion

Implementing two microextrusion-based 3D bioprinting methods facilitated the fabrication of 3D constructs to be employed as pH sensors and drug-releasing components in a developed wound dressing. Use of hydrogels in this fabrication system benefited the final wound dressing through fast diffusion of water-soluble molecules which is also accommodated by the porosity of the 3D printed structures. This diffusion behavior is useful for drug delivery and pH sensing application which will be discussed in the next chapter. Characterization of two adapted 3D printing methods enabled the fabrication of hydrogel structures with required fiber diameter through control over material deposition rate and printing speed. Printability assay also determined the feasible printing zones in terms of alginate and crosslinking agent concentration.

Chapter Three: Development of a Multifunctional, Hydrogel-Based Wound Dressing

As discussed in previous chapters, bacterial infection has a detrimental impact on the wound healing process, in which case, preventive measures against infection or its early detection can be noted as an absolute necessity. Dire consequences of wound infection include delayed healing rate, increased treatment cost, and mortality. Based on this, development of a wound dressing with the ability to inhibit bacterial growth and detect bacterial infection can facilitate the wound healing process (Boateng & Catanzano 2015; Dargaville et al. 2013).

In this project, a hydrogel-based wound dressing with embedded pH sensors and drug-releasing components was developed to enable the colourimetric measurement of wound pH – an indicator of bacterial infection – and delivery of antimicrobial agents to the wound site. The transparent hydrogel dressing allowed for detection of bacterial infection without a need for dressing removal and exposing the wound to the environment, reducing the chance of infection and inflicted pain to the patient. The hydrogel patch – made of alginate and glycerol – afforded the required flexibility to maintain a conformal contact with the wound as indicated in Figure 3-1.

Alginate is a natural polysaccharide with extensive applications in biomedical science and engineering. Having favorable biocompatibility and simple gelation process, alginate hydrogel has become a suitable biomaterial choice in wound healing, drug delivery, and tissue engineering applications (Lee & Mooney 2012). Wound dressings, made of alginate hydrogel, preserve the wound moisture and facilitate the wound healing (Queen et al. 2004). Alginate dressings can also be used in dried form, in which case, they absorb

the wound exudate and re-gel due their high hydrophilicity and supply the moisture to the dry wound afterwards. This property controls the wound secretion and has been shown to promote granulation tissue formation and rapid epithelization (Boateng et al. 2008; Lee & Mooney 2012).

Furthermore, the addition of glycerol – a simple biocompatible polyol and a plasticizer – to the wound dressing material has been reported to enhance the mechanical properties of the fabricated dressings (Liakos et al. 2014; Thu et al. 2012; Dallan et al. 2007). These mechanical properties include increased elasticity and reduced rigidity which are essential characteristics of a dressing to endure mechanical loading and provide a conformal contact with the wound surface.

The aforementioned pH sensors were fabricated by the 3D bioprinting of alginate hydrogel using the coaxial extrusion system (discussed in Chapter 2). In these sensors, alginate hydrogel was loaded with anion-exchange beads which were previously coated with Brilliant Yellow or cabbage juice as halochromic dyes. Brilliant Yellow as a synthetic pH indicator (Tamayol et al. 2016; Egawa et al. 2006) and cabbage juice as a natural material containing pH-sensitive pigment (Chigurupati et al. 2002) were immobilized on the anion-exchange beads in the pH sensors and their colour change based on the variation of acidity enabled the pH measurement.

In the developed system, the acidity of the wound dressing environment was measured by implementing colourimetry and image processing techniques for tracking the colour change of pH sensors. In this system, an array of pH sensors – with the potential to be tuned based on the wound shape and geometry – were employed to map the bacterial infection in different regions of the wound. The use of colourimetry facilitated the *in situ*

wound monitoring, creating a potential for integration with a smartphone application for image processing and determining the wound pH in a real-time manner.

Drug-releasing components were also fabricated with 3D bioprinting method. For this purpose, the single-channel extrusion system (discussed in Chapter 2) was employed to form antibiotic-loaded alginate hydrogels. Gentamicin was used as the antimicrobial agent in the fabricated drug-loaded components. It is a broad-spectrum antibiotic with the bactericidal effect on both gram-negative and gram-positive bacteria. This antimicrobial agent can irreversibly bind with the bacterial ribosome and interrupt their protein synthesis (Woodcock et al. 1998). This *in situ* drug delivery can accommodate the required concentration of antibiotic at the infected region with reduced serum level of the drug and, therefore, reduced side effects compared to the condition of systemic administration by injection or oral use (Langer 1980).

The developed hydrogel patch had the potential to be integrated with a Mepitel® film – a commercial wound dressing – and make a compound wound dressing. The incorporation of Mepitel® film enabled a better attachment between the dressing and the skin while reducing the water vapor permeability and preserving the wound moisture to enhance the healing rate.

The functionality of the developed wound dressing in terms of detecting bacterial infection was assessed by conducting an *ex vivo* test on infected pig skin samples. The potential to inhibit bacterial growth was evaluated based on the impact of the dressing on *P. aeruginosa*, a common type of bacterium in epidermal wounds. Furthermore, several properties of the hydrogel dressing including pH response time, moisture preservation, dehydration rate, and hydration rate were characterized.

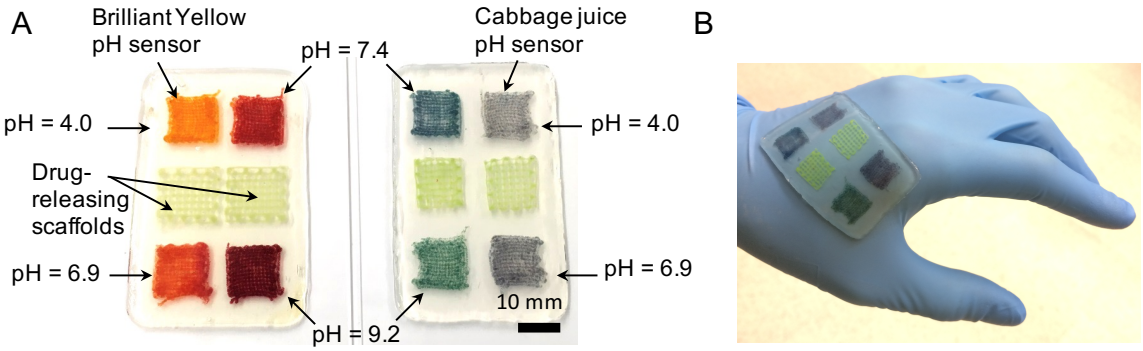

Figure 3-1- A) Developed wound dressing with pH sensors and antibiotic-leaded components. Brilliant Yellow (left) and cabbage juice (right) were used as the pH sensitive dyes. B) The dressing was made of alginate hydrogel with 1.5 mm of thickness and had the required flexibility to follow the curvature of its substrate.

3-1- Materials and methods

Preparation of Brilliant-Yellow- and cabbage-juice-loaded beads: 6 ml of anhydrous ethanol was used to dissolve 135 mg of Brilliant Yellow dye (TCI, Tokyo, Japan). The dye solution was mixed with 24 ml of DI water and stirred for 30 minutes. For the preparation of cabbage juice, 15g of chopped red cabbage was added to 30ml of DI water and incubated at 90ºC for 1 hour. The resultant mixture was filtered with filter papers (Whatman™, UK), and stored at 4ºC. Both pH-responsive dyes (Brilliant Yellow solution and cabbage juice) were coated on Dowex 1x4 chloride form (Sigma, St. Louis, USA) – anion exchange beads. This process started with adding 3378 mg of Dowex beads to 50 ml of DI water in a 50ml Falcon® tube, then the suspension was manually shaken and incubated at room temperature for 15 minutes until the beads were fully settled at the bottom of the tube. The water content was replaced by pipetting – three times with DI water and finally with anhydrous ethanol. After removing ethanol from the suspension, 30 ml of DI water was added to the beads, shaken manually, and then added

to the dye solution – Brilliant Yellow solution or cabbage juice – for obtaining two types of pH-responsive beads. The final suspension was stirred for 2 minutes at room temperature and washed multiple times with DI water according to the previous washing steps to have a clear supernatant which was finally extracted from the suspension. Coated beads were then suspended in alginate solution before 3D printing process.

Preparation of printing materials for pH sensors: For 3D printing pH sensors, alginate solution in DI water was used as the printing material. Sodium alginate (Sigma, St. Louis, USA) was added to 15 ml of DI water to reach a certain concentration. The initial mixture was stirred at 60°C for 1 hour to have a homogeneous solution. Previously prepared pH-sensitive beads were suspended in alginate solution and vortex-mixed at 3000 rpm prior to use in the 3D printing process.

Preparation of printing materials for drug-releasing scaffolds: The proper amount of gentamicin sulfate (Sigma, USA) – determined by the desired drug content in the final scaffold – was added to 5 ml of DI water and vortex-mixed for 1 minute. Sodium alginate (Sigma, St. Louis, USA) was then added to drug solution to achieve the desired concentration. For preparing alginate solution with a concentration of 6% (w/v) or less, a similar procedure as discussed for pH sensitive solution was followed. For alginate solution with higher concentration (10% (w/v) and 16% (w/v)), the mixture was incubated at 60 °C and stirred manually with a glass bar to create a uniform paste. The paste was degassed in a vacuum chamber with -30 PSI of gauge pressure for 15 minutes afterward.

Fabrication of pH sensors and drug-releasing scaffolds: 3D printing was used for fabrication of pH sensors and drug releasing scaffolds by coaxial microfluidic and single-

channel extruder systems, respectively. Fabrication and characterization of 3D printed fibers were performed according to the discussed methods in the previous chapter. Fabrication process, pH sensors, and drug-releasing scaffolds are shown in Figure 3-2.

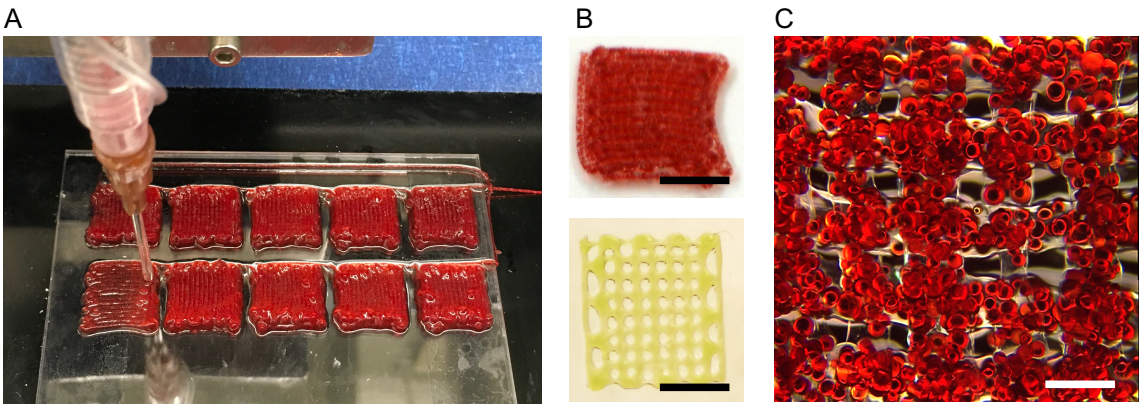

Figure 3-2- A) Fabrication process of pH sensors, using microextrusion 3D printing. B) Fabricated pH sensors (top) and drug-releasing scaffolds (bottom). Scale bar: 5 mm. C) Microscopic image of a pH sensor with embedded pH-responsive beads. Scale bar: 1 mm.

Colourimetric assessment of pH sensors: As indicated in Figure 3-3 A, pH sensors changed colour based on the acidity of their environment. For characterizing this colour change and correlating to the pH value of the sensors' environment, a light box was used for photography of pH sensors, as shown in Figure 3-3 B. These photographs were then post-processed with ImageJ – an image processing software. Image processing was performed by splitting red/green/blue (RGB) channels of the photos and determining the gray-scale intensity of each channel. Using an 8-bit grayscale for the images, 256 (2^8) levels of luminance per pixel were provided for each channel, 0 being black and 255 being white.

A

pH	4.0	7.4	9.2
Brilliant yellow	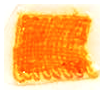	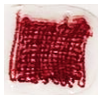	
Cabbage juice	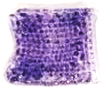	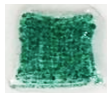	

B

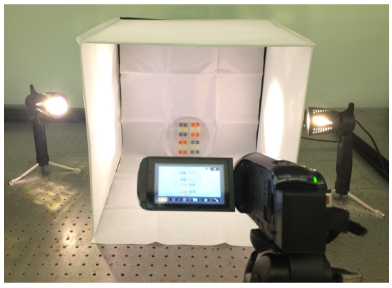

Figure 3-3- A) Brilliant Yellow and cabbage juice pH sensors gain different colours based on the acidity of their environment. B) The light box that was used for photography of pH sensors in buffers with different acidities.

Fabrication of wound dressings: Wound dressings were composed of pH sensors and drug releasing scaffolds, embedded in a hydrogel patch. The patch was made of alginate or alginate-glycerol hydrogels. Table 3-1 shows the materials composition of different patches.

Material composition					
Alginate (%w/v)	2	4	6	2	2
Glycerol (%v/v)	0	0	0	20	40

Table 3-1- Material composition of different fabricated patches made of alginate and glycerol

Alginate solution was prepared according to the previously discussed method. Glycerol (Anachemia, USA) was added to alginate solution, incubated at 60°C for 30 minutes, and vortex-mixed multiple times to have a homogeneous solution. Hydrogel patches were fabricated using a Plexiglas mold with four cuboid cavities with dimensions of 35 mm×55 mm×1.5 mm, as shown in Figure 3-4. Each cavity was filled with sodium alginate or sodium alginate-glycerol solution in which the previously fabricated pH sensors and drug-releasing scaffolds were submerged. For each patch, 4 pH sensors were

inserted at the corners along with two drug-loaded scaffolds at the center. In the next step, the hydrogel was formed by placing an agarose hydrogel sheet – made of 1% (w/v) agarose and 4% (w/v) calcium chloride in DI water – on top of each cavity. The mold was incubated for two hours at room temperature to allow sodium alginate to ionically crosslink.

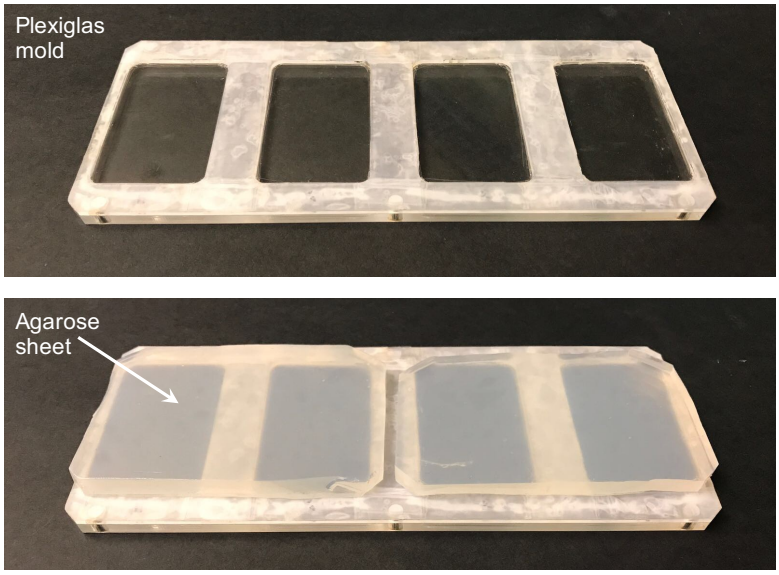

Figure 3-4- A Plexiglas mold was used for fabrication of wound dressings (top). Agarose hydrogel (bottom) with 5 mm of thickness contained the crosslinking agent and was placed on top of the mold which was filled with alginate or alginate- glycerol solution.

Determination of pH response time: pH response time of sensors and wound dressings with different material composition were evaluated by exposing them to different buffers and changing the acidity of their environment from the neutral condition. The previously mentioned light box was used for continuous imaging of sensors and dressings, and the time required for sensors to reach a steady state condition in terms of their colour was considered as the pH response time.

Determination of the water vapor transmission rate (WVTR): The WVTR of hydrogel sheets with different material compositions, according to Table 3-1, was measured by the previously developed Modified Cup Method (Mukhopadhyaya et al. 2005). For this purpose, a testing device was designed and manufactured, as indicated in Figure 3-5. The modified cup device consisted of a water chamber, a sample holder, and a desiccant chamber. A piece of filter paper was attached to the desiccant chamber to separate the desiccant – 2 gr of calcium chloride – from the hydrogel sample. Circular hydrogel samples with 9/16" of diameter and 1.5 mm of thickness were inserted between water and desiccator chambers to separate two environments with 100% and 0% of relative humidity, respectively. The inner environment of the device was sealed with an O-ring, and the desiccant chamber was removable for periodic weighing during the experiment. The amount of water vapor – transmitted through the hydrogel – was calculated by measuring the gained weight in the desiccant chamber and using Eq. 1.

$$WVTR\ (gr.m^{-2}.day^{-1}) = \frac{(\Delta W_{desiccant})}{A} \times 24 \qquad \text{Eq. 1}$$

In which, $\Delta W_{desiccant}$ is the weight change of the desiccant chamber in gr after 1 hour and A is the hydrogel sample area.

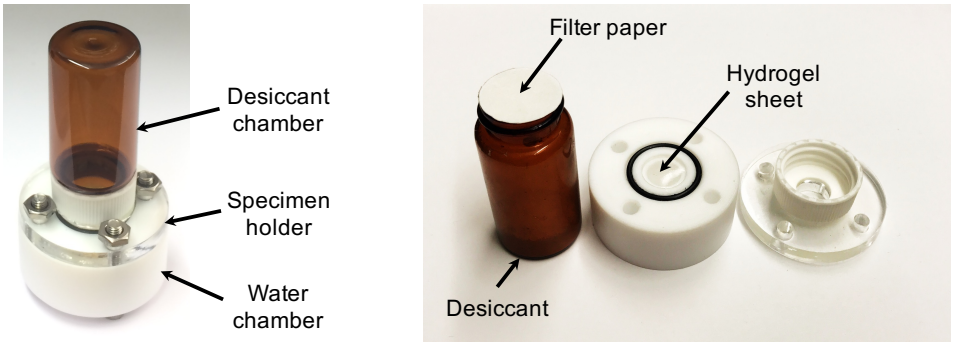

Figure 3-5- Developed device for determining the WVTR of hydrogel sheets with different material composition. The device was composed of a desiccant chamber on top, a sample holder, and a water chamber at the bottom.

Dehydration test: Dehydration rate was determined for hydrogel sheets with different material compositions and thicknesses. Square 15 mm × 15 mm gel sheets made of different concentration of alginate and glycerol and two different thickness, 1.5 mm and 3 mm, were fabricated by a similar method as discussed for the fabrication of the dressings. Samples were air-dried at room temperature, while weight measurement at certain times during the experiment determined their dehydration rate according to Eq. 2.

$$RW\ (\%) = \frac{W_i - W}{W_i} \times 100 \qquad \text{Eq. 2}$$

Where, RW is the remaining weight percentage, W_i is the initial weight of the sample, and W is the weight of the sample at each time points.

Hydration rate: The hydration behavior of polymeric samples was evaluated by hydrating freeze-dried sheets with the same material and thickness which were used for the dehydration test samples. Hydrogel sheets were fabricated according to the previously discussed procedures, incubated at -80°C overnight, and freeze-dried for 24 hours. Samples were weighed at the beginning of the experiment and submerged in 0.1 M Tris (Sigma, St. Louis, USA) buffer (pH 7.4). Degree of swelling for submerged samples was calculated by weight measurement at certain time points and using the following equation.

$$S\ (\%) = \frac{W - W_i}{W_i} \times 100 \qquad \text{Eq. 3}$$

In this equation, S is the gained weight percentage, W_i is the initial weight of the sample, and W is the weight of the sample at each time points.

Incorporation of the Mepitel®: As shown in Figure 3-6, a Mepitel® film – a commercial wound dressing with the capability of use in combination with other dressings – was incorporated into the developed hydrogel wound dressing to enhance its

attachment to the skin, reduce its WVTR, and prolong its longevity by reducing the dehydration rate.

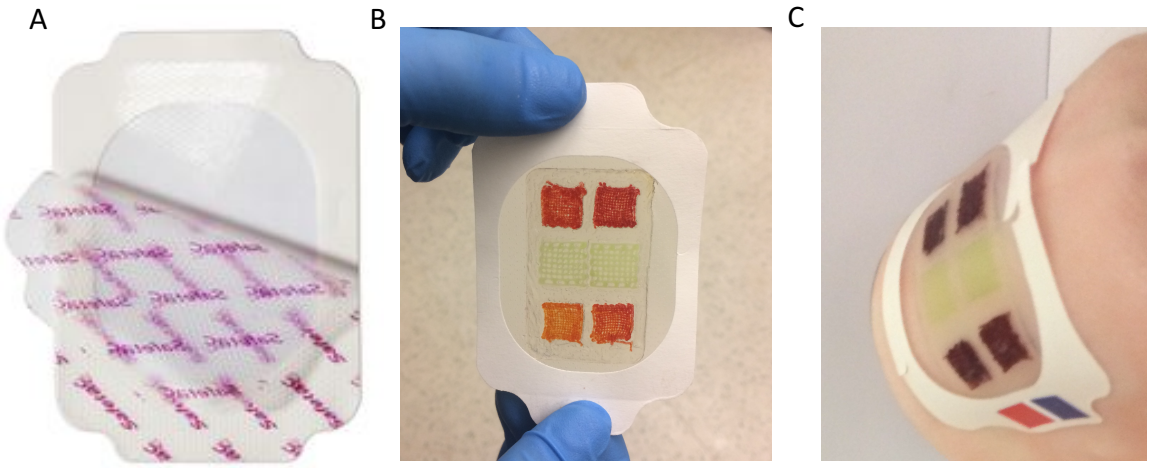

Figure 3-6- A) Mepitel® film, a commercial wound dressing. B) Hydrogel wound dressing attached to a Mepitel® film. C) The final wound dressing was able to follow the curvature of the skin and had an effective attachment. The image shows the compound wound dressing on a pig skin sample.

WVTR and dehydration tests were also repeated for hydrogels samples with an attached Mepitel® film and the results were compared to the experimental results obtained from hydrogels alone.

Bacteria culture: *P. aeruginosa* – American Type Culture Collection (ATCC) 10145 – was cultured in Tryptic Soy Broth (TSB) (Becton, Dickinson) overnight at 37°C while shaking at 200 rpm. After diluting 1:10 in sterile saline, it was swabbed on a Tryptic Soy Agar (TSA) plate to create a lawn. *S. aureus* was isolated at the University of Victoria and grown with the same method as mentioned for *P. aeruginosa*.

To observe the colour change in pH sensors in the case of bacterial infection, they were exposed to the by-products of mentioned strains of bacteria. 1 ml of the supernatant obtained from bacterial culture medium was collected at hourly time points and their pH

was measured by pH probe. 150 μl of collected supernatant was dropped on pH sensors and their colour change was evaluated by the image processing method. Subsequently, measured pH with pH probe was compared with the pH value derived from pH sensors.

Bacteria viability loss test: The functionality of drug-loaded scaffolds was assessed by embedding fabricated gentamycin-loaded scaffolds into hydrogel patches and placing them on the lawn of *P. aeruginosa* on TSA plates using sterile forceps. The TSA plates were incubated overnight at 37°C, and bacterial growth was determined by post-culture of the swabs taken from proximity of the drug-loaded hydrogel to a new TSA plate.

***Ex-vivo* test:** To evaluate the functionality of the wound dressing in detecting the bacterial infection, an *ex vivo* test was conducted on pig skin samples. For this assay, edible pig skin was purchased from a supermarket (Fairway Market, Victoria, Canada), cut into square 7 cm × 10 cm pieces, and sterilized with 70% ethanol. Then, *P. aeruginosa* with 3 different densities of $1.4\times10^5\ cfu/cm^2$, $1.4\times10^6\ cfu/cm^2$, and $1.4\times10^7\ cfu/cm^2$ was cultured on the pig skin samples. Subsequently, wound dressings were placed on top of the infected pig skins and the colour change of pH sensors was investigated after 30 minutes.

3-2- Results and discussion

The developed wound dressings were characterized and assessed in terms of different characteristics and functionalities, including pH responsiveness, hydration and dehydrations rates, WVTR, ability to detect bacterial infection, and the capability to inhibit bacterial growth.

Imaging and image processing were used to characterize the colour change of pH sensor. For this purpose, the gray-scale intensity of RGB channels was determined for both types of pH sensors (Brilliant Yellow and cabbage juice) in environments with different pH values, as shown in Figure 3-7.

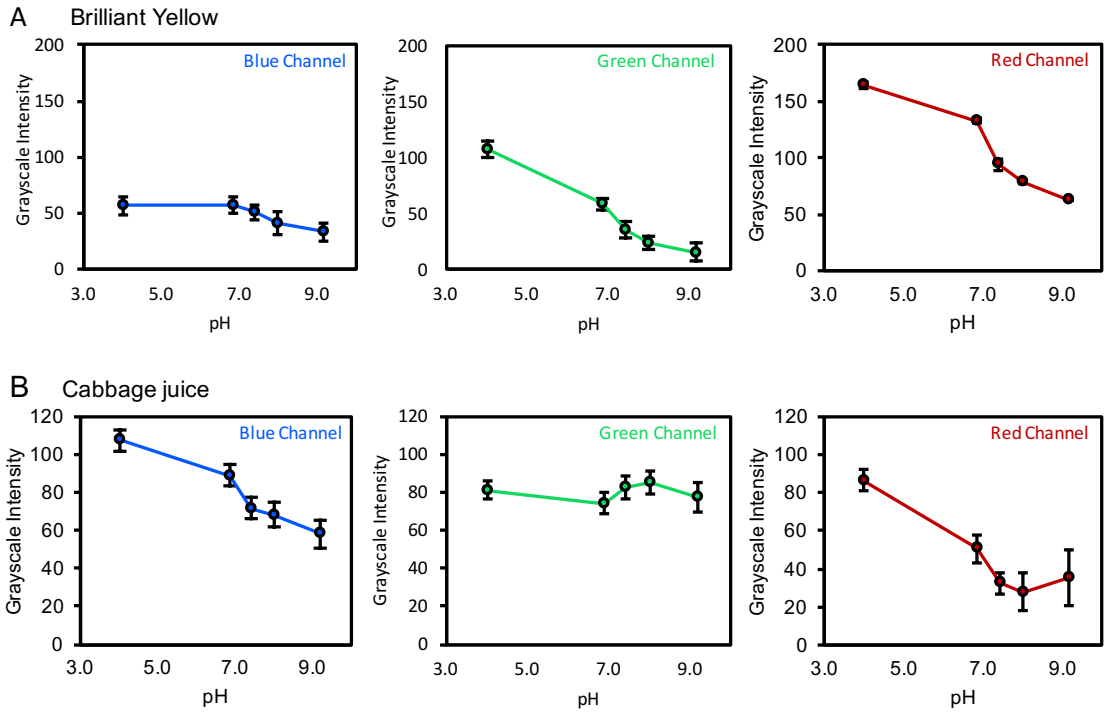

Figure 3-7- A) Variation of RGB gray-scale intensities for Brilliant Yellow (A) and cabbage juice (B) pH sensors in environments with different acidity. Error bars are SD (n=3).

For Brilliant Yellow sensors, the red channel had the largest variation of gray-scale intensity, and therefore, was considered as the basis for determination of pH value. In contrast, cabbage juice had its largest variation of gray-scale intensity in the blue channel, by which pH value was determined. For this purpose, two standard equations – correlating pH value to the gray-scale intensity – were derived based on fitted curves (Figure 3-8) on red and blue channel data points.

- Red channel – Brilliant Yellow:

$$y = -1.61\times10^{-5}x^3 + 5.23\times10^{-3}x^2 - 5.67\times10^{-1}x + 28.7 \qquad \text{Eq. 4}$$

- Blue channel – cabbage juice

$$y = -1.12\times10^{-4}x^3 + 2.70\times10^{-2}x^2 - 2.20x + 68.2 \qquad \text{Eq. 5}$$

In these equations, x indicates the gray scale intensity and y serves as pH value, enabling an output of acidity value based on the input from sensors' images. This phenomenon enables the integration of the wound dressing with a smartphone application for monitoring the wound condition in a real-time manner.

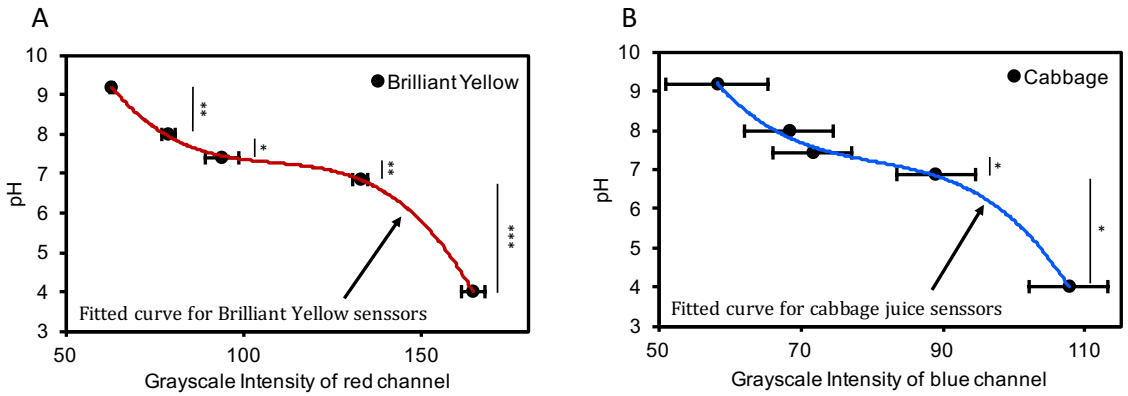

Figure 3-8- Standard curves correlate pH value to gray scale intensity of photographs taken from sensors in environments with different acidity. Red channel was used for Brilliant Yellow sensors (A), and blue channel was used for sensors containing cabbage juice. Error bars are SD (n=3). * P<0.05, ** P<0.005, and *** P<0.0005.

Derived polynomial formulas facilitate the interpretation of colourimetry for quantitative pH measurement. Moreover, a uniform trend and larger variation in gray-scale intensity allows for a larger tolerance in dependence on background lighting and leads to a more accurate pH measurement.

The response time of individual pH sensors with different content of alginate – 2% (w/v) to 6% (w/v) – was determined for both types of sensors, containing Brilliant Yellow and cabbage juice. Figure 3-9 shows a typical gray-scale intensity variation versus time for sensors with 4% (w/v) alginate in response to different ranges of pH change. It was observed that an acidic condition triggered a larger colour variation

compared to the basic condition, and Brilliant Yellow had a broader intensity change in comparison with cabbage juice. Cabbage juice by changing from purple to pale green from acidic to the basic condition had a more noticeable colour change to the human eye, while Brilliant Yellow changed colour from orange to dark red. Considering the fact that pH 4 led to larger variation in gray-scale intensity and had the slowest response time, all of the response time characterizations occurred in this pH value.

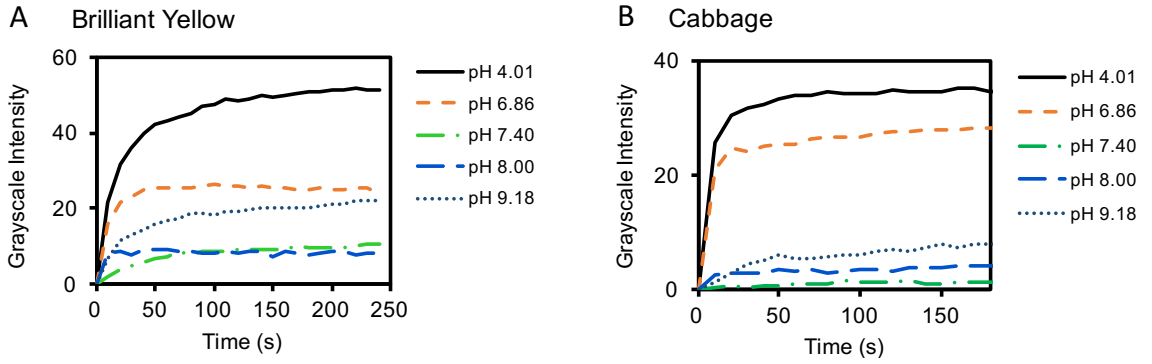

Figure 3-9- Response time of pH sensors made of 4% (w/v) alginate containing (A) Brilliant yellow and (B) cabbage juice in different ranges of pH change from neutral condition. In both tests n=3.

The impact of several parameters including the alginate concentration in the sensors and in the patch, patch thickness, patch porosity, the introduction of glycerol, and printed fibers' diameter was investigated. Since pH responsiveness is a diffusion-based phenomenon, any factor that delays the diffusion of molecules from the environment to the sensors prolongs the required time for reaching equilibrium condition, and therefore, creates a slower response. Based on this, increasing the concentration of alginate in the sensors from 2% (w/v) to 6% (w/v) resulted in an increase in response time from 155±10 and 105±10 seconds to 285±10 and 315±10 seconds for Brilliant Yellow and cabbage juice sensors, respectively. Similarly, enlarging the printed fibers' diameter from 550 μm to 650 μm approximately doubled the response time. Using gel sheets instead of 3D

printed sensors also increased the response time from less than 200 seconds to more than 600 seconds for both types of sensors. Gel sheets were made of the same material and contained the same amount of pH indicator – Brilliant Yellow and cabbage juice. The influence of mentioned factors regarding pH sensors on the response time is shown in Figure 3-10.

Moreover, evaluating the response time of pH sensors with two different porosity –3D printed structures and gel sheets – evidenced the positive contribution of 3D printing method to a faster response, resulting in a faster infection diagnosis. Considering all effective factors, sensor's porosity had the most significant effect on pH response time by enhancing the response rate more than 3 times.

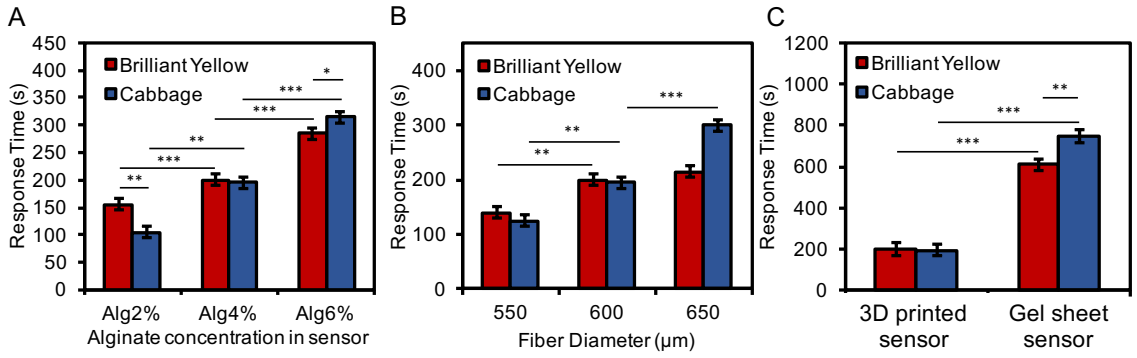

Figure 3-10- The effect of different parameters on the response time of pH sensors containing Brilliant Yellow and cabbage juice, including concentration of alginate (A), printed fibers' diameter (B), and sensors' porosity (C). The effect of porosity was assessed by evaluating the response time of gel sheet sensors and comparing with the results obtained from 3D printed sensors. Error bars are SD (n=3). * P<0.05, ** P<0.005, and *** P<0.0005.

pH response time was also influenced by different parameters in the hydrogel patch, namely, patch thickness, alginate concentration in the patch, and the addition of glycerol. As shown in Figure 3-11, by increasing patch thickness from 1.5 mm to 3 mm, response time became slower from 11 and 15 minutes to 35 and 43 minutes for Brilliant Yellow

and cabbage juice sensors. Using a higher concentration of alginate demonstrated a similar outcome since a denser gel network results from a higher polymer content. Incorporation of glycerol led to a slower response time which can be justified by the additional network that glycerol brought to the hydrogel structure.

Alginate with 2% (w/v), 4% (w/v) and 6% (w/v) was used for fabricating hydrogel patches with thickness of 1.5 mm, 2 mm, and 3 mm in characterization experiments, however, dressing with 1.5 mm of thickness made of 2% (w/v) alginate was determined as the optimal condition in terms of pH response time and suitable flexibility. While glycerol content had a detrimental effect on pH response time, its positive impact on the dehydration rate and patches' flexibility in the dried condition made it a suitable additive material. The effect of glycerol will be discussed more in the next sections.

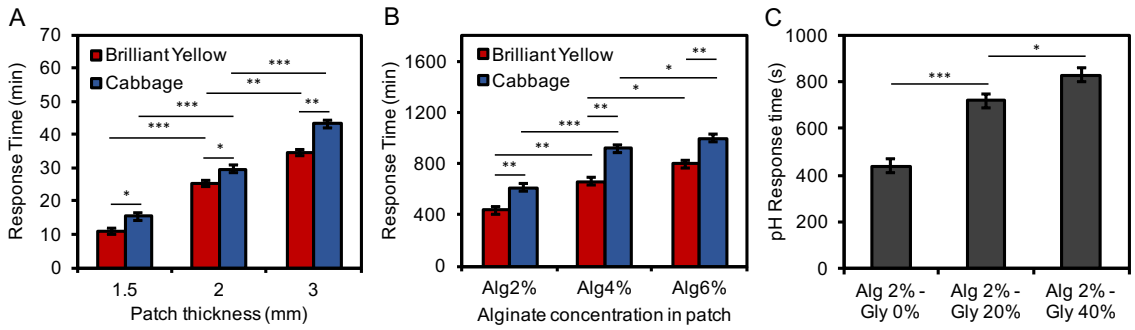

Figure 3-11- The variation of pH response time by altering the patch thickness (A), alginate concentration (B), and incorporating glycerol with concentration of 20% (v/v) and 40% (v/v) (C). Error bars are SD (n=3). * P<0.05, ** P<0.005, and *** P<0.0005.

To study the effect of dressing thickness on its pH response time and justify the regarding experimental results, a numerical simulation was performed in commercially available COMSOL 5.1. as shown in Figure 3-12, hydrogel patch with pH sensors was modeled with a 2-dimensional geometry and different thicknesses according to the experimental samples.

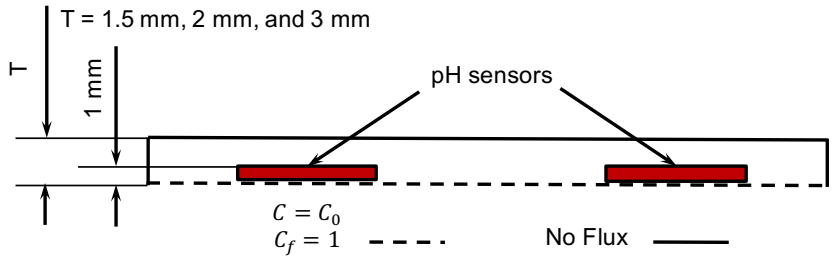

Figure 3-12- Two-dimensional diffusion-based model of the hydrogel patch with pH sensors for determining the effect of patch thickness on pH response time.

Fick's first and second law of diffusion were considered as the governing equations for diffusion phenomenon in hydrogel patches.

$$C_f = \frac{C}{C_0} \quad \text{Eq. 6}$$

$$\mathbf{J} = -D\boldsymbol{\nabla} C_f \quad \text{Eq. 7}$$

$$\frac{\partial C_f}{\partial t} = -\boldsymbol{\nabla}.\mathbf{J} \quad \text{Eq. 8}$$

In these equations, C is the concentration of hydrogen ions in the patch, C_0 is the concentration of hydrogen ions at the wound, C_f is the concentration fraction, $\mathbf{J}$ is the diffusive flux, and D is the diffusion coefficient. Diffusion coefficient was set based on the average experimental diffusion time and was used for all thickness conditions. This consideration for diffusion coefficient accounts for diffusion process and the required time for the pH sensitive dyes to respond to the pH change. Triangular elements were used for discretizing the domain, and the mesh size was decreased until the independence of the solution from the mesh size. The time step was set to 1 second to reach an independent solution of the time steps.

For the numerical simulation, pH response time was defined as the time required to reach a constant concertation of hydrogen ions on the pH sensor's top surface. Since this surface is the visible region in image processing, constant concentration indicates a

steady colour on the pH sensors. The outcome of the numerical simulation appeared to be in agreement with the experimental results. As shown in Figure 3-13, by increasing the patch thickness, pH response time also increased significantly, which can be explained by the effect of extended diffusion distance on the diffusion process. In other words, enlarging the patch thickness created an extra volume of hydrogel on top of the sensors to sink the hydrogen ions and therefore extended the diffusion process.

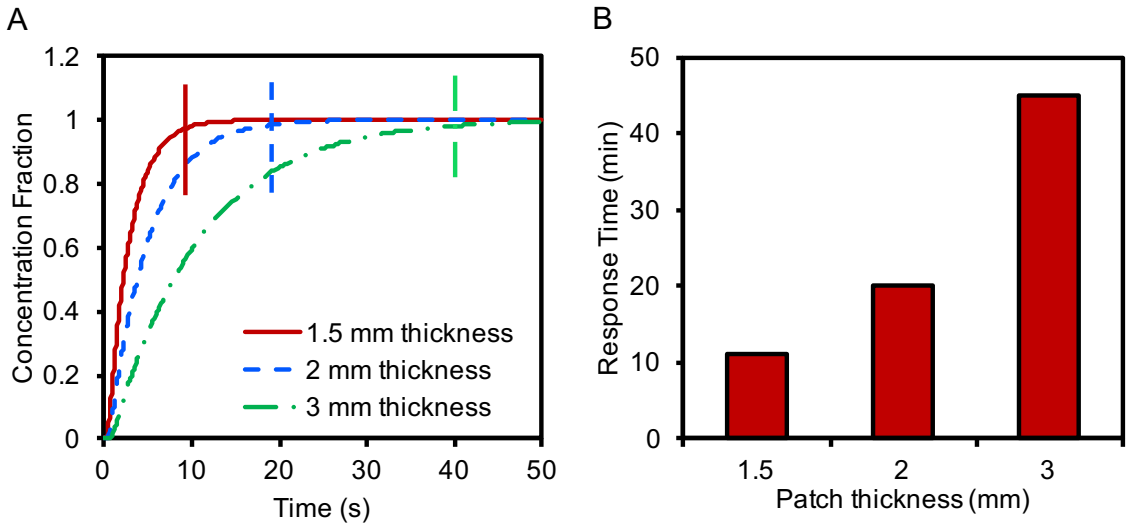

Figure 3-13- Results from the numerical simulation. A) Change in concentration fraction of hydrogen ions over time for patches with different thicknesses. Vertical lines indicate the time points when concentration fraction was considered to remain constant. B) The pH response time variation against the thickness change.

WVTR is one of the crucial properties of wound dressings as it affects the evaporative water loss in the wound. The significance of wound moisture management is based on the fact that negative consequences can result from either wound dehydration or build-up of exudate underneath the wound dressing due to high or low WVTR, respectively. High WVTR in hydrogel dressings leads to the dehydration and shrinkage of the hydrogel and exposure of the wound edges to the environment (Queen et al. 1987). On the other hand, exudate build-up – as a result of low WVTR – may cause clinical issues including

creation of a back pressure due to the high resistance to the water transport, leakage of exudate and maceration of surrounding healthy skin tissue, and dislocation of the dressing and exposure of the wound edges to the environment. Table 3-2 summarizes the reported WVTR for several previously developed dressings a few of which have become commercial.

Dressing	Thickness (mm)	WVTR ($g.m^{-2}.day^{-1}$)	Reference
Geliperm (agar and polyacrylamide)	1.13 ± 0.19	10973 ± 998	(Queen et al. 1987)
Vigilon (cross-linked polyethylene oxide and polyethylene)	0.03	9360±34	(Balakrishnan et al. 2005)
Oxidized alginate and gelatin	4.2	2686±124	
Chitosan-alginate polyelectrolyte complex	0.024 - 0.026	623.6 ± 28.3 - 764.8 ± 32.0	(Wang et al. 2002)
Bilayer hydrocolloid alginate film	3.14 ± 0.04	5280 ± 240	(Thu et al. 2012)
Single-layer hydrocolloid alginate film	0.69 ± 0.02	13440 ± 240	

Table 3-2- Water vapor transmission rate (WVTR) of several reported or commercial wound dressings.

The WVTR test was conducted on the developed hydrogel wound dressing alone and in combination with a Mepitel® film. As shown in Figure 3-14, individual hydrogel patches with different material composition – alginate hydrogel and alginate-glycerol hydrogel – appeared to have similar WVTR – from 8253±1167 $gr.m^{-2}.day^{-1}$ to 9078±1184 $gr.m^{-2}.day^{-1}$ for alginate 2% (w/v) and alginate 2% (w/v) combined with 40% (v/v) glycerol, respectively. In Contrast, incorporation of Mepitel® film significantly reduced the WVTR to 2218±52 $gr.m^{-2}.day^{-1}$ due to the additional resistance resulted from an extra layer. A range of 2000-2500 $gr.m^{-2}.day^{-1}$ has been reported as a suitable WVTR because it creates twice the resistance of granulation tissue to water vapor transport (Queen et al. 1987).

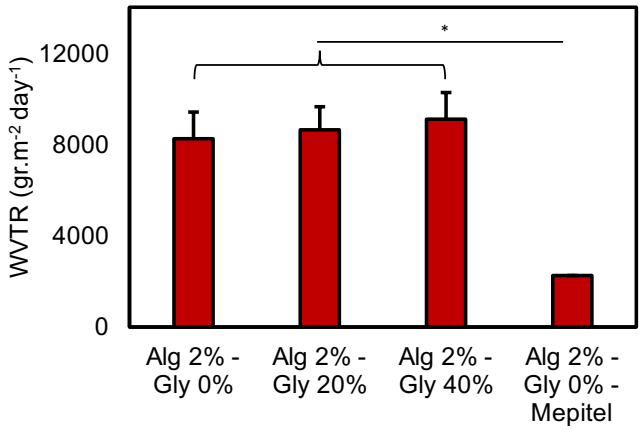

Figure 3-14- WVTR for hydrogel patches with different material compositions and with the incorporation of Mepitel® film. Error bas are SD (n=3). * P<0.05.

Dehydration rate of the dressing was evaluated by experimentation on alginate hydrogel patches with different concentration of alginate and different thicknesses. Remaining weight of the hydrogel samples during air-drying under room conditions over time indicated the effect of hydrogel thickness and alginate concentration on dehydration behavior. As shown in Figure 3-15, increase in thickness of the hydrogel patch from 1.5 mm to 3 mm and alginate concentration from 2% (w/v) to 4% (w/v) delayed the complete

dehydration time from 8 hours to 24 hours, in which case, the former factor appeared more effective.

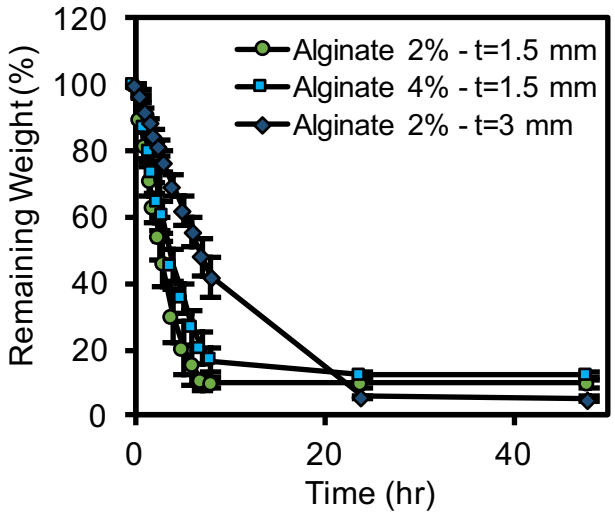

Figure 3-15- Dehydration of hydrogel patched with different content of alginate and different thicknesses over time. Error bars are SD (n=4).

The dehydration rate of the hydrogel indicates its longevity in the practical situation. A long dehydration time affords a longer duration of use on the skin as the dressing can preserve its moisture content and maintain minimized shrinkage.

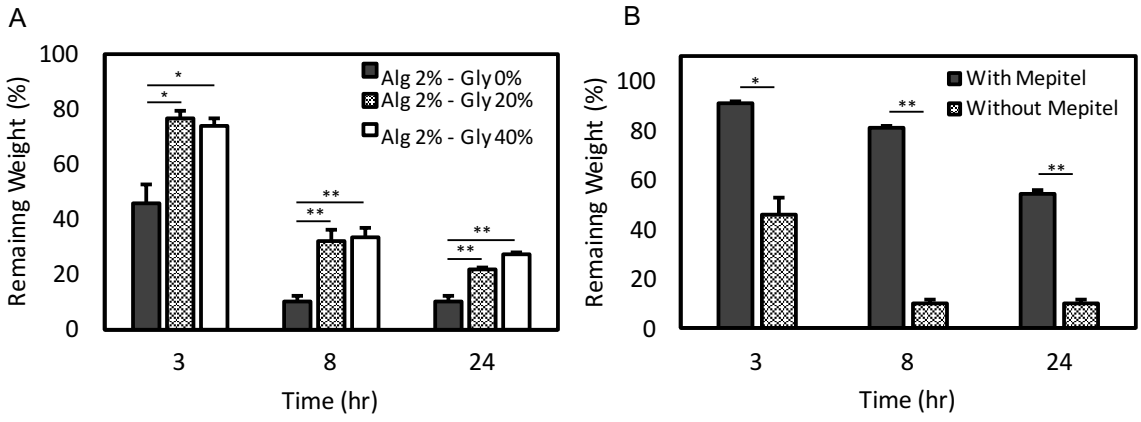

Figure 3-16- A) Remaining weight of the hydrogel patches with and without glycerol content in different time points. B) The effect of Mepitel® film on the dehydration of the wound dressing. * P<0.05 and ** P<0.005. Error bars are SD (n=4).

The effect of glycerol and the additional Mepitel® layer on dehydration rate was also determined. As shown in Figure 3-16 A, incorporation of glycerol to the hydrogel leads to a reduced dehydration rate, as the remaining hydrogel weight increases from 10%±1.8% for alginate 2% (w/v) without glycerol to 21.4%±0.6% and 27.4%±0.7% with addition of 20 % (v/v) and 40 % (v/v) glycerol, respectively, after 24 hour of air-drying.

The addition of the Mepitel® film also increased the remaining weight of the hydrogel patch at different time points during the dehydration process. As indicated in Figure 3-16 B, there is a significant difference between the remaining weight of hydrogel patch alone – 10%±1.8% – and the compound dressing made of hydrogel patch and Mepitel film – 54.3%±1.6% – after 24 hours.

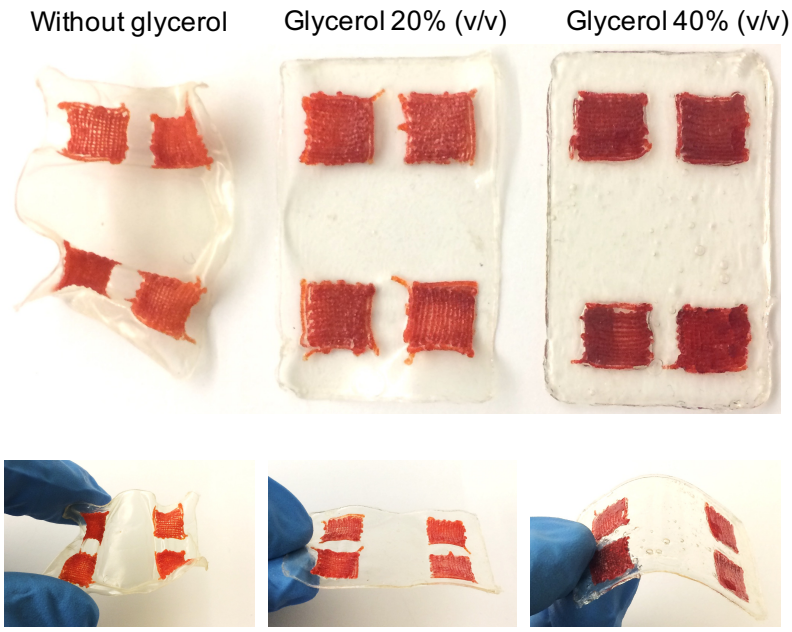

Figure 3-17- Glycerol reduced the shrinkage and deformation and enhanced the flexibility of the hydrogel patches in dehydrated form. Photos were taken after 24 hours of air-drying at room temperature.

In addition to the effect on the dehydration rate, glycerol reduced the shrinkage and deformation of the fabricated wound dressing considerably while enhanced its flexibility,

as shown in Figure 3-17. Deformation and shrinkage may result in the breakdown of bacterial barrier – as one of the main functions of a wound dressing – by wound edge exposure. On the other hand, loss of flexibility may inhibit the conformal contact of the dressing with the wound surface.

The developed wound dressings can be stored and distributed to the consumer in freeze-dried form and hydrated prior to use. For this reason, the hydration behavior of the dried patch is an important factor in determining the required duration of hydration for retaining the maximum water content. Figure 3-18 shows the freeze-dried dressings with different material composition, alginate 2% (w/v) alone, with 20 % (v/v) of glycerol, and with 40 % (v/v) of glycerol. Similar to air-dried dressings, glycerol content enhanced the flexibility in freeze-dried condition, which is a positive effect as it reduces the potential for damage prior to hydration.

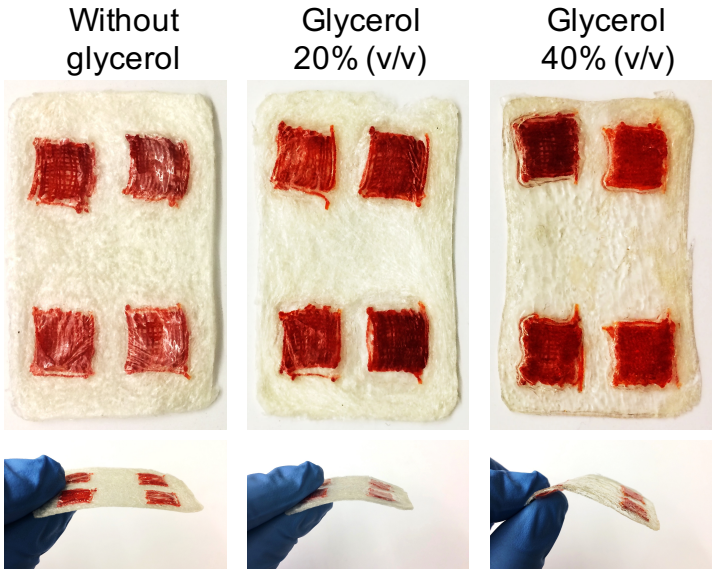

Figure 3-18- Freeze-dried dressings with different material compositions. Glycerol increased the flexibility of freeze-dried wound dressings.

The degree of swelling was determined over time for patches with two different concentration of alginate – 2% (w/v) and 4% (w/v) – and two different thicknesses, 1.5

mm and 3 mm. As demonstrated in Figure 3-19, in all conditions, freeze-dried wound dressings absorbed their maximum water content after 2.5 hours.

The addition of glycerol was observed to significantly reduce the degree of swelling from 269±62% for hydrogels without glycerol to 25.2%±1.3% and 21.5%±1.8% with 20% (v/v) and 40% (v/v) of glycerol.

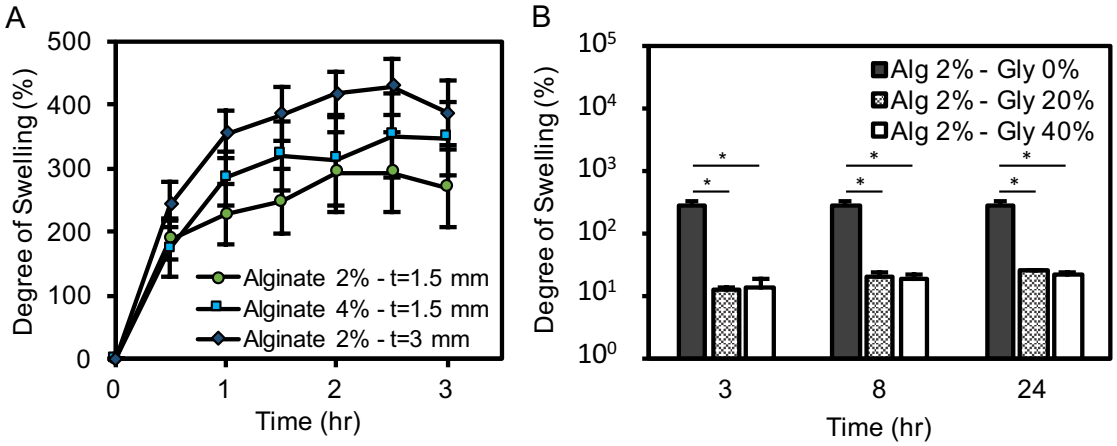

Figure 3-19- Degree of swelling for patches with different material compositions and thicknesses (left) and the effect of glycerol on hydration rate of the dressing (right). * P<0.005. Error bars are SD (n=4).

The acidity of bacteria by-products was determined, over time, for both types of bacteria. This assay allowed for determining the correlation of bacterial growth and pH of their supernatant. As indicated in Figure 3-20 A, *P. aeruginosa* has an increasing trend in its pH over time as it started from 6.5, turned to slightly basic condition after 2 hours, and reached over 9 after 8 hours of culture. In contrast, *S. aureus* had acidic by-products, starting from a neutral condition and ending with the pH of about 6 after 8 hours of growth, as shown in Figure 3-20 B.

The previously mentioned types of bacteria are very common in epidermal wounds, and typically, burn wounds. Experimentation with these two types enabled the assessment of the functionality of pH sensors in both acidic and basic conditions.

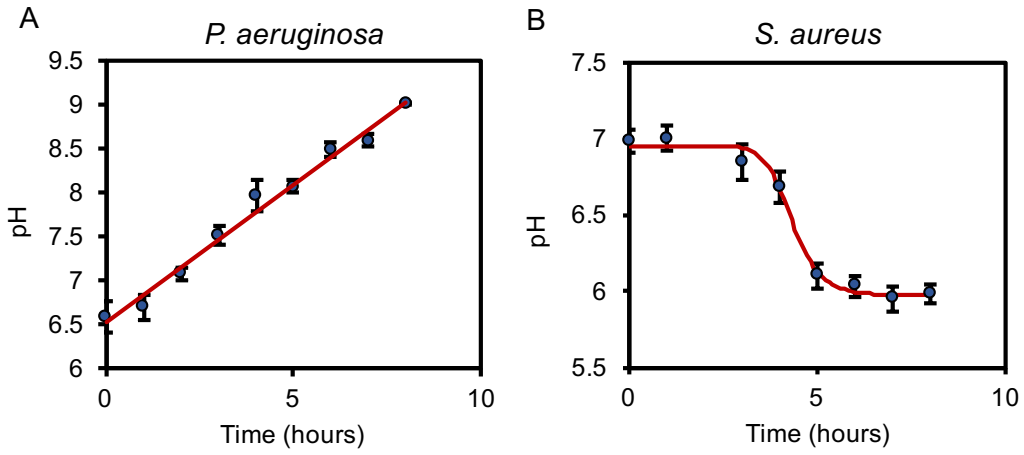

Figure 3-20- Acidity of bacteria by-products, measured by a pH probe, during their growth time for (A) *P. aeruginosa* and (B) *S. aureus*. Error bars are SD (n=3).

By putting the bacteria supernatant, obtained from different times of growth from 1 hour to 8 hours, a gradient of colour change was observed for both types of pH sensors. Exposure to *P. aeruginosa* led Brilliant Yellow pH sensors to change colour from dark orange to dark red, as shown in Figure 3-21. On the other hand, cabbage juice sensors had a lower degree of colour variation from pale to dark green.

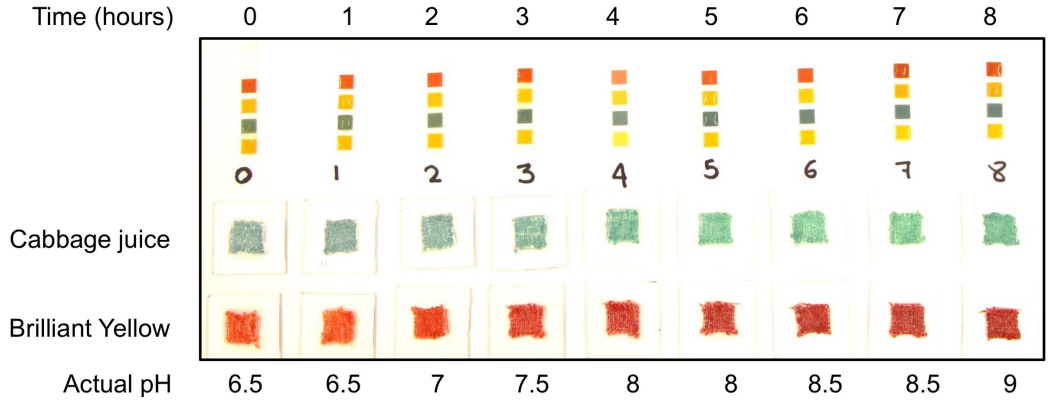

Figure 3-21- Colour change of pH sensors as a result of the exposure to the by-products of *P. aeruginosa*. Brilliant Yellow sensors showed more observable colour change compared to cabbage juice sensors.

The acidity of the bacteria supernatants was measured by two types of sensors – based on image processing – and was compared to the actual pH, measured by pH probe. As

shown in Figure 3-22, pH of the bacteria by-products was evaluated with a higher accuracy by Brilliant Yellow sensors, having errors below 6% of the actual pH value. This error of measurement was less than 9% for cabbage juice sensors.

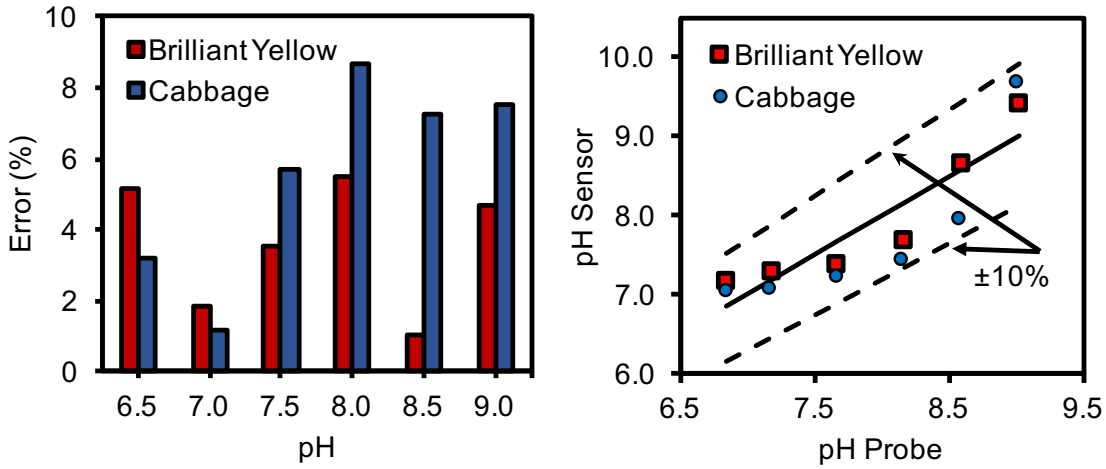

Figure 3-22- The acidity of *P. aeruginosa* supernatants was measured by both types of pH sensors, and the error of measurement was determined. Measurement with Brilliant Yellow sensors led to a higher accuracy compared to cabbage juice sensors.

Figure 3-23 demonstrates the colour change of sensors containing cabbage juice and Brilliant Yellow exposed to the by-products of *S. aureus*. Brilliant Yellow had a lower colour change from red to dark orange, while cabbage juice changed colour from steel blue to purple. In contrast to the basic condition, cabbage juice sensors demonstrated a more visible colour change in exposure to acidic bacteria by-products.

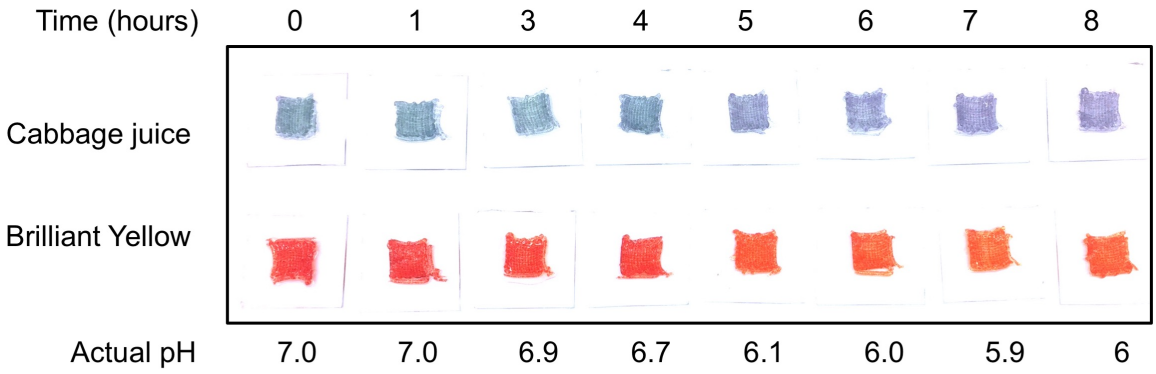

Figure 3-23- The effect of *S. aureus* supernatant on pH sensors over time.

As opposed to the colour change, Brilliant Yellow sensors led to a higher accuracy in pH measurement with errors of less than 6% of the actual pH value, in comparison with cabbage juice sensors with errors of below 14 %. Figure 3-24 shows the error of pH measurement in different pH values.

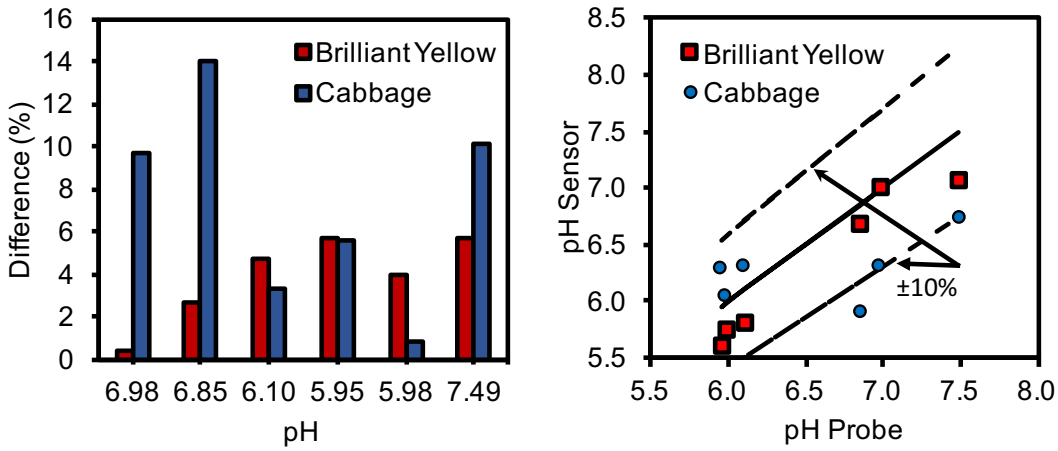

Figure 3-24- The error of pH measurement with two types of pH sensors exposed to the supernatant of *S. aureus*. Brilliant Yellow showed a more accurate measurement compared to cabbage juice sensors, however, the error of both types remained under 10% of the actual pH value, except for one data point with 14% error for cabbage juice sensors.

Overall, pH sensors containing Brilliant Yellow provided a higher accuracy in pH measurement. This can be explained by the fact that Brilliant Yellow is a synthetic material with a higher product consistency. On the other hand, cabbage juice in pH sensors represented a more noticeable colour change from acidic to basic condition, making it a suitable choice for applications without image processing.

Drug-loaded scaffolds in the wound dressing showed promising impact on the lawn of *P. aeruginosa* on TSA plates. As represented in Figure 3-25, hydrogel patches containing different amount of gentamicin sulfate, from 50 μg to 300 μg, were tested, among which antibiotic content of 200 μg and 300 μg resulted in a considerable removal of green pigment. This green pigment was produced by *P. aeruginosa.* To ensure the inhibition of

bacterial growth, three different regions around the hydrogel with 200 μg of antibiotic were post-cultured on another TSA plate (Figure 3-25 C), and region 1 demonstrated no considerable bacterial colony. As seen in Figure 3-25 D, removal of bacterial green pigment – or the growth inhibition zone – showed a considerable extension around the hydrogels with higher antibiotic content (300 μg).

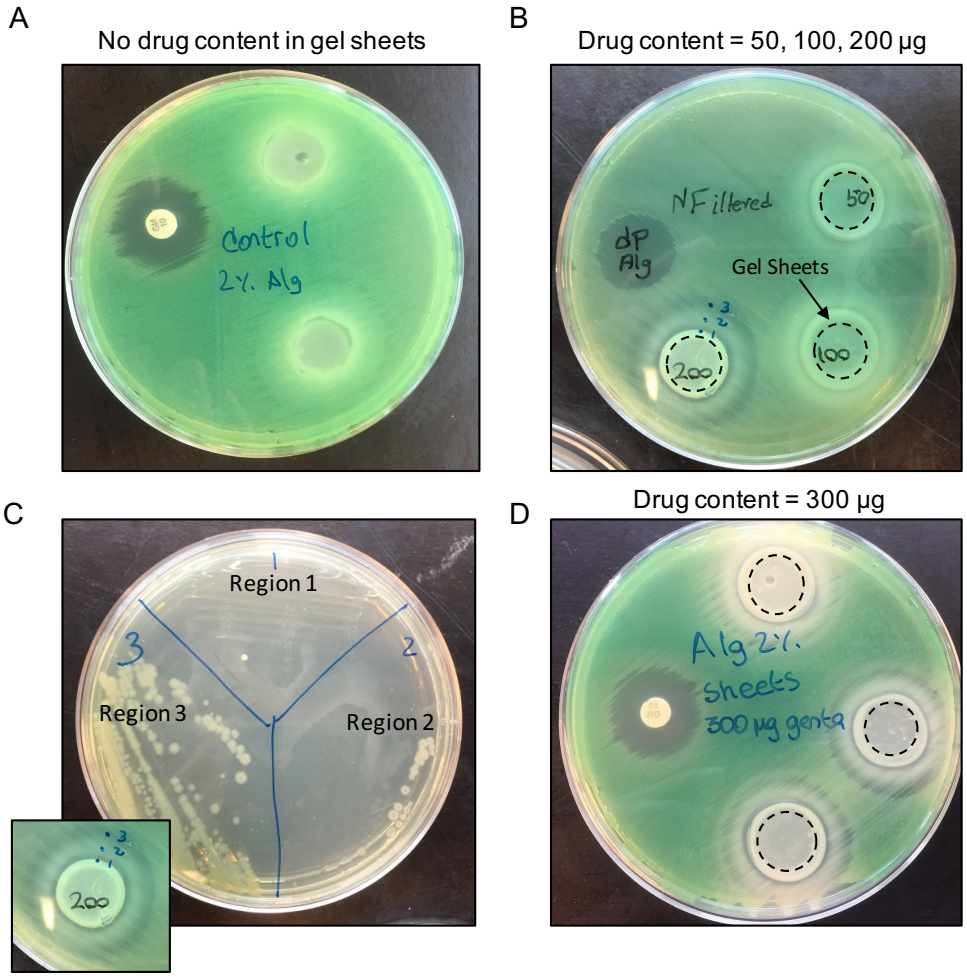

Figure 3-25- Hydrogel patches with different content of gentamicin sulfate on the lawn of *P. aeruginosa* on TSA plates. (A) Control condition with no content of antibiotic. (B) Drug-loaded condition with 3 different contents of gentamicin sulfate from 50 to 200 μg. Dashed lines show the edge of the hydrogels and surrounding white regions have resulted from the removal of green pigment produced by *P. aeruginosa*. (C) Three different regions around the hydrogel patch containing 200 μg of gentamicin sulfate were post-cultured on another

TSA plate and no considerable bacteria colony was observed in region 1. (D) hydrogel patches with 300 μg of gentamicin sulfate on TSA plate led to an extended inhibition zone.

This *in situ* drug delivery can be implemented with different water-soluble antimicrobial agents, individually or in compound forms, and lead to a reduced drug dosage in the bloodstream, minimizing the resultant side effects.

Drug-loaded hydrogel patches were sterilized by UV irradiation prior to the aforementioned experiment. UV exposure time was characterized by applying different UV duration from 5 minutes to 30 minutes and culturing swabs – taken from the hydrogels – on TSA plates. As represented in Figure 3-26, 30 minutes of UV exposure led to an effective sterilization since no considerable bacterial growth was detected on the TSA plate.

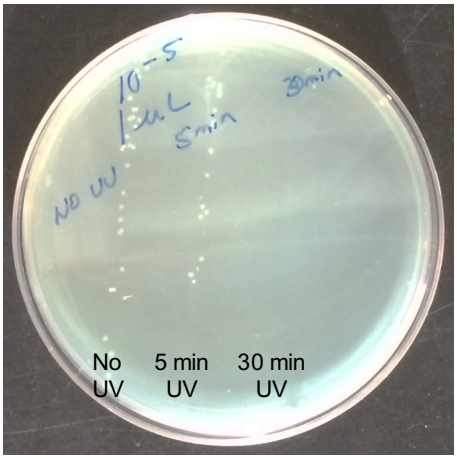

Figure 3-26- Culture of swabs taken from sterilized drug-loaded hydrogels. 30 minutes of UV exposure showed an effective sterilization with no considerable bacteria on the TSA plate.

The functionality of the wound dressing in detecting bacterial infection was assessed by an *ex-vivo* assay on infected pig skins. *P. aeruginosa* was cultured on initially non-contaminated pig skin samples with three different density – from $1.4\times10^5\ cfu/cm^2$ to $1.4\times10^7\ cfu/cm^2$ – as demonstrated in Figure 3-27.

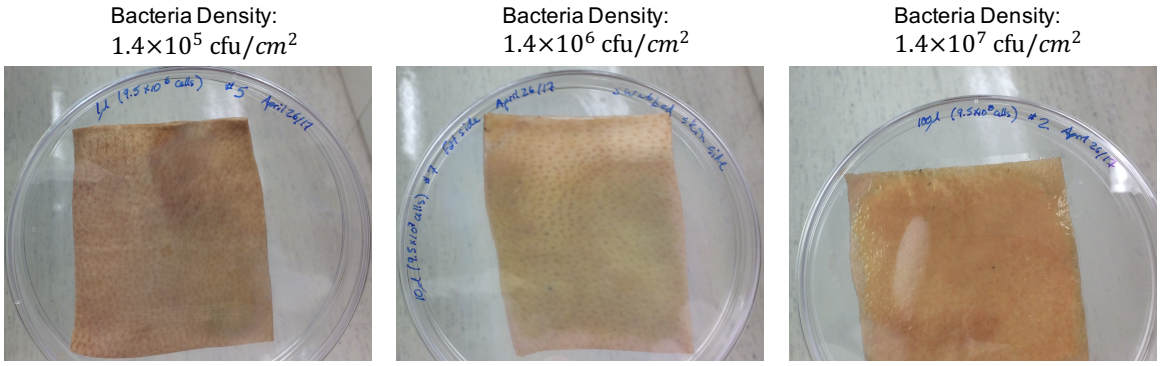

Figure 3-27- Pig skin sample with cultured *P. aeruginosa* in three different densities. Photos are taken after bacteria culture overnight.

As seen in Figure 3-28, this assay illustrated that pH sensors acquired a trend of colour change – based on the bacteria density – on infected pig skin samples. This phenomenon can be explained by the fact that pH is a function of bacteria population (Figure 3-29 A), enabling the correlation of degree of colour change to the infection severity.

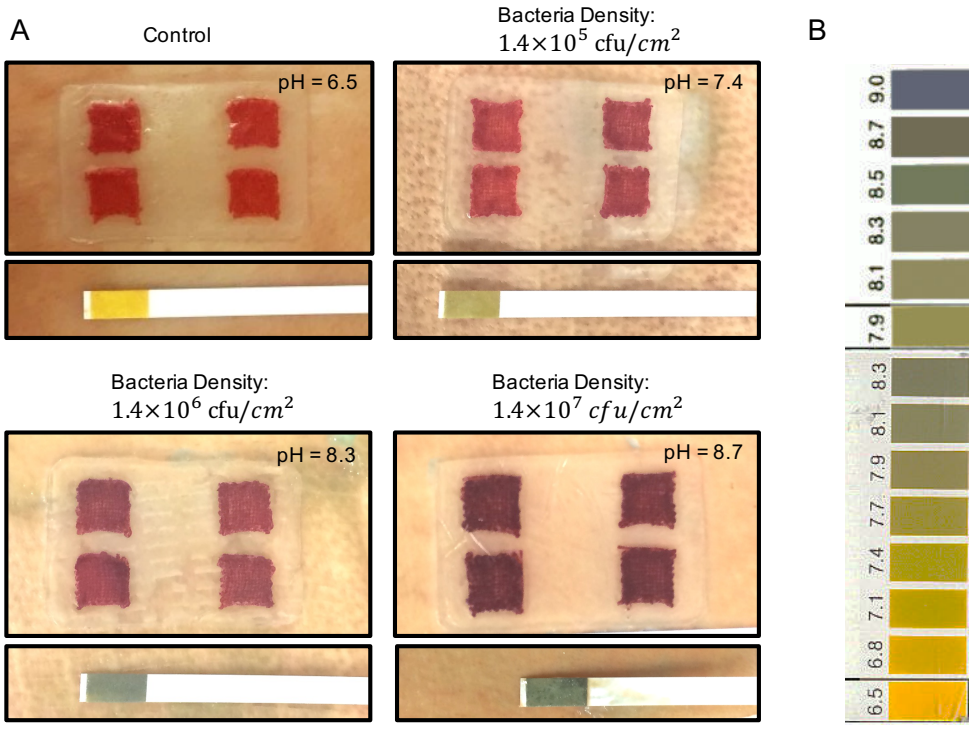

Figure 3-28- A) Wound dressings with Brilliant Yellow pH sensors on pig skin samples – contaminated with different density of *P. aeruginosa*. pH sensors showed a trend of colour

change according to the bacteria density after 30 minutes of incubation. B) Reference colours for pH strips.

Furthermore, the pH of pig skin samples was measured by pH sensors and compared to the value derived from pH strips. Results showed a promising measurement accuracy with deviations within the 5% of actual pH value, as demonstrated in Figure 3-29 B.

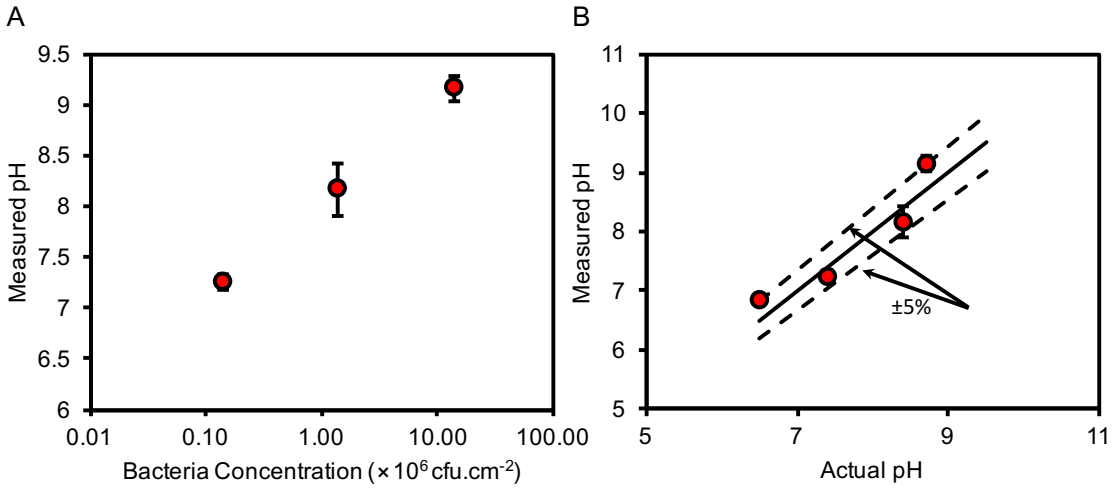

Figure 3-29- (A) pH of the pig skins based on the density of bacterial infection. (B) The error of pH measurement with Brilliant Yellow pH sensors based on the deviation from measurement by pH strips. Error bars are SD (n=3).

3-3- Conclusion

The developed wound dressing with the capability of mapping bacterial infection at the wound site – based on the acidity of bacteria by-products – enabled real-time wound monitoring via an image-processing method. Taking advantage of colourimetry method with halochromic materials, the wound dressing provided an *in situ* measurement of pH – as an indicator of bacterial infection – with an array of pH sensors. This system eliminates the need for removing the wound dressing for detecting infection by which the

patients can be subjected to an excessive pain while the exposure of the wound to the environment increases the chance of infection. Introduction of antibiotic-loaded components into the wound dressing provided an *in situ* drug delivery and inhibited the growth of *P. aeruginosa* on TSA plates. Being made of alginate hydrogel, the wound dressing provided a suitably moist environment to prevent wound dehydration and afforded a suitable water vapor transport. The hydrogel patch was able to make a compound wound dressing with Mepitel® film to enhance its attachment to the skin and reduce the WVTR. Both the hydrogel patch and the aforementioned compound dressing had the required flexibility to maintain a conformal contact with the wound. An *ex-vivo* experiment on infected pig skin samples demonstrated the capability of the fabricated wound dressing to determine the severity of infection based on the degree of colour change in its pH sensors. A future direction of this work is developing a pH-sensitive drug delivery system to correlate the antibiotic delivery to the detection of bacterial infection.

Conclusion and Future Direction

Disease demographics show that global health care system has been considerably burdened by the frequent occurrence of epidermal wounds and particularly their susceptibility to infection. Infection in epidermal wounds leads to further medical complications and slow healing rate whose prevention and early diagnosis allow for a more effective wound treatment. Traditional wound care approaches have been appeared incapable of generating an optimal healing condition in terms of maintaining wound moisture, provision of an effective microorganism barrier, and early detection of wound infection. Mentioned drawbacks have led to the emergence of recent wound care methods especially for the treatment of chronic and burn wounds.

Many recent approaches toward inhibiting infection in epidermal wounds have been focused on the development of impregnated wound dressing by the incorporation of antimicrobial agents such as antibiotics and silver. The inclusion of silver has been repeatedly implemented in commercial wound dressings and extensively explored in the scientific literature. Silver in different chemical compositions, and more recently, silver nanoparticles have been shown to affect a wide range of microorganisms including bacteria and fungi. Specifically, silver is a suitable antimicrobial alternative for eradicating antibiotic-resistant strains of bacteria. However, its cytotoxicity can negatively affect fibroblasts and macrophages which are the essential cellular components during the wound healing process. Alternatively, antibiotics can affect a narrower spectrum of microorganisms while posing reduced toxicity to human cells. Additionally, *in situ* delivery of antibiotics to the wound significantly minimizes the level

of these drugs in the serum compared to the condition of systemic administration, reducing their side effects.

Wound monitoring – particularly for detecting infection – have traditionally been performed with culture-based methods such as culture of wound swabs and specimens obtained from tissue biopsy. While affording the quantitative assessment of microorganisms present at the wound, complications regarding these methods and their required incubation time prevent real-time wound monitoring. Based on this, alternative sensing methods have been developed to monitor the wound condition either in point-of-care diagnostic systems or in integrated forms with wound dressings. These sensing platforms employ various involving factors including wound temperature, wound acidity, wound odour, and several microorganism by-products as indicators of infection. Various techniques such as electrochemical sensing and colourimetry have been utilized to monitor aforementioned infection indicators. Among these techniques, the use of electrochemical sensors is limited due to a need for power supply in some cases – for integration with the wound dressing – and electrode failure in wound environment. Alternatively, pH sensing by mean of colourimetric and image processing methods offers a great potential for integration of infection sensors with wound dressing, accommodating real-time and *in situ* wound monitoring.

This thesis proposed a multifunctional hydrogel-based wound dressing with the ability to inhibit and detect bacterial infection in epidermal wounds. This wound dressing comprised of pH sensors and drug-loaded hydrogel constructs, fabricated by microextrusion-based 3D bioprinting. Gentamicin hydrochloride as a broad-spectrum antibiotic – affecting both gram-negative and gram-positive bacteria by disrupting their

protein synthesis – was encapsulated in the 3D bioprinted hydrogels to prevent bacterial growth. Incorporation of this antibiotic into alginate hydrogel sheets showed a great promise in inhibiting the growth of *P. aeruginosa* on TSA plates. In the developed wound dressing, infection monitoring was enabled by an array of pH sensors containing halochromic dyes, Brilliant Yellow and cabbage juice. An image processing method was employed for determining the wound pH based on the photos taken from the dressing. The developed method obviated the need for dressing removal in detecting infection which is necessary for implementing the traditional methods. While both pH-sensitive dyes demonstrated a promising potential for detecting *P. aeruginosa* and *S. aureus in vitro*, Brilliant Yellow offered a higher accuracy and cabbage juice, in most cases, showed a more observable colour change. An *ex-vivo* test – conducted on infected pig skin samples with *P. aeruginosa* – showed a colour change in dressings with Brilliant Yellow sensors according to the bacterial density. The hydrogel dressing was integrated with a Mepitel® film – a commercial wound dressing – to provide an effective attachment with the skin and reduce the overall WVTR. This property along with the high water content in the hydrogel enabled a prolonged dehydration time, suitable for maintaining the wound moisture and aiding the wound healing process.

As a future direction to this work, the developed wound dressing can be tested *in vivo* on animal models. Other types of antimicrobial agents – such as silver, antimicrobial peptides, and bacteriolytic enzymes – can also be incorporated into the developed wound dressing, and their effect can be investigating by testing on bacterial non-bacterial infections. Moreover, as the addition of biological agents such as growth factors has been shown to provide therapeutic effects and facilitate the wound healing process, this feature

can be included in the wound dressing and its impact can be determined on fibroblasts and keratinocytes. A connection between the drug delivery system and pH sensing can accommodate a smart drug-release based on the presence of microorganisms. Furthermore, the determination of the shelf-life of this product will provide a valuable information for its production and storage.

Bibliography

Anon, 1989. Transparent hydrogel wound dressing. Available at: https://www.google.com/patents/US5106629 [Accessed June 23, 2017].

Aoyagi, S., Onishi, H. & Machida, Y., 2007. Novel chitosan wound dressing loaded with minocycline for the treatment of severe burn wounds. *International Journal of Pharmaceutics*, 330(1–2), pp.138–145. Available at: http://linkinghub.elsevier.com/retrieve/pii/S0378517306007393 [Accessed June 25, 2017].

Balakrishnan, B. et al., 2005. Evaluation of an in situ forming hydrogel wound dressing based on oxidized alginate and gelatin. *Biomaterials*, 26(32), pp.6335–6342. Available at: http://www.sciencedirect.com/science/article/pii/S0142961205003194 [Accessed May 10, 2017].

Barbetta, A. et al., 2014. Rapid Prototyping of Chitosan-Coated Alginate Scaffolds Through the Use of a 3D Fiber Deposition Technique. *Journal of Materials Chemistry B*, 2, pp.6779–6791. Available at: http://pubs.rsc.org/en/Content/ArticleLanding/2014/TB/C4TB00732H.

Bindu, T.V.L.H. et al., 2011. Preparation and evaluation of gentamicin loaded chitosangelatin composite films for wound healing activity. *International journal of applied biology and pharmaceutical technology*, 2, pp.453–463. Available at: http://imsear.li.mahidol.ac.th/handle/123456789/161522 [Accessed June 30, 2017].

Boateng, J. & Catanzano, O., 2015. Advanced Therapeutic Dressings for Effective Wound Healing?A Review. *Journal of Pharmaceutical Sciences*, 104(11), pp.3653–3680. Available at: http://www.ncbi.nlm.nih.gov/pubmed/26308473 [Accessed June 25, 2017].

Boateng, J.S. et al., 2008. Wound Healing Dressings and Drug Delivery Systems: A Review. *Journal of Pharmaceutical Sciences*, 97(8), pp.2892–2923. Available at: http://linkinghub.elsevier.com/retrieve/pii/S0022354916326521 [Accessed June 28, 2017].

Boateng, J.S., Pawar, H. V. & Tetteh, J., 2013. Polyox and carrageenan based composite film dressing containing anti-microbial and anti-inflammatory drugs for effective wound healing. *International Journal of Pharmaceutics*, 441(1–2), pp.181–191. Available at: http://linkinghub.elsevier.com/retrieve/pii/S0378517312010526 [Accessed June 25, 2017].

Chen, D.W. et al., 2012. Sustainable release of vancomycin, gentamicin and lidocaine from novel electrospun sandwich-structured PLGA/collagen nanofibrous membranes. *International Journal of Pharmaceutics*, 430(1–2), pp.335–341. Available at: http://linkinghub.elsevier.com/retrieve/pii/S0378517312003560 [Accessed July 1, 2017].

Cheng, X. et al., 2013. Revealing silver cytotoxicity using Au nanorods/Ag shell nanostructures: disrupting cell membrane and causing apoptosis through oxidative damage. *RSC Advances*, 3(7), p.2296. Available at: http://xlink.rsc.org/?DOI=c2ra23131j [Accessed July 8, 2017].

Chigurupati, N. et al., 2002. Evaluation of red cabbage dye as a potential natural colour

for pharmaceutical use. *International Journal of Pharmaceutics*, 241(2), pp.293–299.

Chopra, I. & Roberts, M., 2001. Tetracycline antibiotics: mode of action, applications, molecular biology, and epidemiology of bacterial resistance. *Microbiology and molecular biology reviews : MMBR*, 65(2), p.232–60 ; second page, table of contents. Available at: http://www.ncbi.nlm.nih.gov/pubmed/11381101 [Accessed June 26, 2017].

Church, D. et al., 2006. Burn Wound Infections. *Clinical Microbiology Review*, 19(2), pp.403–434.

Cozzarelli, N.R., 1977. THE MECHANISM OF ACTION OF INHIBITORS OF DNA SYNTHESISl. *Ann. Rev. Biochem*, 46, pp.641–68. Available at: http://www.annualreviews.org/doi/pdf/10.1146/annurev.bi.46.070177.003233 [Accessed June 26, 2017].

Dallan, P.R.M. et al., 2007. Effects of chitosan solution concentration and incorporation of chitin and glycerol on dense chitosan membrane properties. *Journal of Biomedical Materials Research Part B: Applied Biomaterials*, 80B(2), pp.394–405. Available at: http://doi.wiley.com/10.1002/jbm.b.30610 [Accessed July 13, 2017].

Dargaville, T.R. et al., 2013. Sensors and imaging for wound healing: A review. *Biosensors and Bioelectronics*, 41, pp.30–42. Available at: http://linkinghub.elsevier.com/retrieve/pii/S0956566312006355 [Accessed June 26, 2017].

Egawa, Y., Hayashida, R. & Anzai, J., 2006. Multilayered assemblies composed of brilliant yellow and poly(allylamine) for an optical pH sensor. *Analytical sciences : the international journal of the Japan Society for Analytical Chemistry*, 22(8), pp.1117–9.

Gemmell, C.G. et al., 2006. Guidelines for the prophylaxis and treatment of methicillin-resistant Staphylococcus aureus (MRSA) infections in the UK. *Journal of Antimicrobial Chemotherapy*, 57(4), pp.589–608. Available at: https://academic.oup.com/jac/article-lookup/doi/10.1093/jac/dkl017 [Accessed June 26, 2017].

Gottrup, F., 2004. A specialized wound-healing center concept: importance of a multidisciplinary department structure and surgical treatment facilities in the treatment of chronic wounds. *The American Journal of Surgery*, 187(5), pp.S38–S43. Available at: http://linkinghub.elsevier.com/retrieve/pii/S0002961003003039 [Accessed June 28, 2017].

Harding, K.G., Morris, H.L. & Patel, G.K., 2002. Healing chronic wounds. *BMJ (Clinical research ed.)*, 324(7330), pp.160–3. Available at: http://www.ncbi.nlm.nih.gov/pubmed/11799036 [Accessed July 11, 2017].

Hospital Corpsman, 2003. First Aid Equipment, Supplies, Rescue, and Transportation. In *Naval Education and Training Command*. pp. 3–1. Available at: http://medical.tpub.com/14295/css/Chapter-3-First-Aid-Equipment-Supplies-Rescue-And-Transportation-115.htm [Accessed June 25, 2017].

Hull, C.W., 1986. Apparatus for production of three-dimensional objects by stereolithography.

Hwang, M.-R. et al., 2010. Gentamicin-loaded wound dressing with polyvinyl alcohol/dextran hydrogel: gel characterization and in vivo healing evaluation. *AAPS*

PharmSciTech, 11(3), pp.1092–103. Available at: http://www.ncbi.nlm.nih.gov/pubmed/20607628 [Accessed June 30, 2017].

Jannesari, M. et al., 2011. Composite poly(vinyl alcohol)/poly(vinyl acetate) electrospun nanofibrous mats as a novel wound dressing matrix for controlled release of drugs. *International journal of nanomedicine*, 6, pp.993–1003. Available at: http://www.ncbi.nlm.nih.gov/pubmed/21720511 [Accessed June 30, 2017].

Jansen, B. et al., 1994. In vitro Evaluation of the Antimicrobial Efficacy and Biocompatibility of a Silver-Coated Central Venous Catheter. *Journal of Biomaterials Applications*, 9(1), pp.55–70. Available at: http://jba.sagepub.com/cgi/doi/10.1177/088532829400900103 [Accessed June 26, 2017].

Järbrink, K. et al., 2016. Prevalence and incidence of chronic wounds and related complications: a protocol for a systematic review. *Systematic reviews*, 5(1), p.152. Available at: http://www.ncbi.nlm.nih.gov/pubmed/27609108 [Accessed July 11, 2017].

Jones, A. V & Cross, N.C.P., 2004. Oncogenic derivatives of platelet-derived growth factor receptors. *Cellular and molecular life sciences : CMLS*, 61(23), pp.2912–23. Available at: http://www.ncbi.nlm.nih.gov/pubmed/15583853 [Accessed June 29, 2017].

Jones, V., Grey, J.E. & Harding, K.G., 2006. Wound dressings. *BMJ (Clinical research ed.)*, 332(7544), pp.777–80. Available at: http://www.ncbi.nlm.nih.gov/pubmed/16575081 [Accessed June 25, 2017].

Kang, H.-W. et al., 2016. A 3D bioprinting system to produce human-scale tissue constructs with structural integrity. *Nature Biotechnology*, 34(3), pp.312–319. Available at: http://www.nature.com/doifinder/10.1038/nbt.3413 [Accessed December 30, 2016].

Klueh, U. et al., 2000. Efficacy of silver-coated fabric to prevent bacterial colonization and subsequent device-based biofilm formation. *Journal of Biomedical Materials Research*, 53(6), pp.621–631. Available at: http://doi.wiley.com/10.1002/1097-4636%282000%2953%3A6%3C621%3A%3AAID-JBM2%3E3.0.CO%3B2-Q [Accessed June 26, 2017].

Knowlton, S. et al., 2015. Bioprinting for cancer research. *Trends in Biotechnology*, 33(9), pp.504–513. Available at: http://www.ncbi.nlm.nih.gov/pubmed/26216543 [Accessed June 23, 2017].

Koch, L. et al., 2012. Skin tissue generation by laser cell printing. *Biotechnology and Bioengineering*, 109(7), pp.1855–1863. Available at: http://www.ncbi.nlm.nih.gov/pubmed/22328297 [Accessed June 23, 2017].

Langer, R., 1980. INVITED REVIEW POLYMERIC DELIVERY SYSTEMS FOR CONTROLLED DRUG RELEASE. *Chemical Engineering Communications*, 6(1–3), pp.1–48. Available at: http://www.tandfonline.com/doi/abs/10.1080/00986448008912519 [Accessed June 25, 2017].

Lazarus, G., Cooper, D. & Knighton, D., 1994. Definitions and guidelines for assessment of wounds and evaluation of healing. *Arch Dermatol*, 130, pp.489–493. Available at: http://jamanetwork.com/data/Journals/DERM/14958/archderm_130_4_015.pdf [Accessed June 28, 2017].

Lee, K.Y. & Mooney, D.J., 2012. Alginate: Properties and biomedical applications. *Progress in Polymer Science (Oxford)*, 37(1), pp.106–126. Available at: http://dx.doi.org/10.1016/j.progpolymsci.2011.06.003.

Levine, N.S. et al., 1976. The quantitative swab culture and smear: A quick, simple method for determining the number of viable aerobic bacteria on open wounds. *The Journal of trauma*, 16(2), pp.89–94. Available at: http://www.ncbi.nlm.nih.gov/pubmed/1255833 [Accessed June 26, 2017].

Liakos, I. et al., 2014. All-natural composite wound dressing films of essential oils encapsulated in sodium alginate with antimicrobial properties. *International Journal of Pharmaceutics*, 463(2), pp.137–145. Available at: http://www.sciencedirect.com/science/article/pii/S0378517313009605 [Accessed July 13, 2017].

Lipsky, B.A. & Hoey, C., 2009. Topical Antimicrobial Therapy for Treating Chronic Wounds. *Clinical Infectious Diseases*, 49(10), pp.1541–1549. Available at: https://academic.oup.com/cid/article-lookup/doi/10.1086/644732 [Accessed July 8, 2017].

Loebl, E.C. et al., 1974. The use of quantitative biopsy cultures in bacteriologic monitoring of burn patients. *Journal of Surgical Research*, 16(1), pp.1–5. Available at: http://linkinghub.elsevier.com/retrieve/pii/002248047490002X [Accessed June 27, 2017].

Luo, Y., Lode, A. & Gelinsky, M., 2013. Direct Plotting of Three-Dimensional Hollow Fiber Scaffolds Based on Concentrated Alginate Pastes for Tissue Engineering. *Advanced Healthcare Materials*, 2(6), pp.777–783. Available at: http://doi.wiley.com/10.1002/adhm.201200303 [Accessed December 30, 2016].

Madhumathi, K. et al., 2010. Development of novel chitin/nanosilver composite scaffolds for wound dressing applications. *Journal of Materials Science: Materials in Medicine*, 21(2), pp.807–813. Available at: http://link.springer.com/10.1007/s10856-009-3877-z [Accessed June 26, 2017].

McLister, A. et al., 2014. Electrochemical approaches to the development of smart bandages: A mini-review. *Electrochemistry Communications*, 40, pp.96–99. Available at: http://linkinghub.elsevier.com/retrieve/pii/S1388248114000113 [Accessed June 27, 2017].

Michael, S. et al., 2013. Tissue Engineered Skin Substitutes Created by Laser-Assisted Bioprinting Form Skin-Like Structures in the Dorsal Skin Fold Chamber in Mice A. T. Slominski, ed. *PLoS ONE*, 8(3), p.e57741. Available at: http://dx.plos.org/10.1371/journal.pone.0057741 [Accessed June 23, 2017].

Mitchell, V., Galizia, J.P. & Fournier, L., 1989. Precise diagnosis of infection in burn wound biopsy specimens. Combination of histologic technique, acridine orange staining, and culture. *The Journal of burn care & rehabilitation*, 10(3), pp.195–202. Available at: http://www.ncbi.nlm.nih.gov/pubmed/2473075 [Accessed June 27, 2017].

Mostafalu, P. et al., 2016. A toolkit of thread-based microfluidics, sensors, and electronics for 3D tissue embedding for medical diagnostics. *Microsystems & Nanoengineering*, 2, p.16039. Available at: http://www.nature.com/articles/micronano201639 [Accessed August 15, 2017].

Mukhopadhyaya, P., Kumaran, M. & Lackey, J., 2005. Use of the Modified Cup Method

to Determine Temperature Dependency of Water Vapor Transmission Properties of Building Materials. *Journal of Testing and Evaluation*, 33(5), p.12507. Available at: http://www.astm.org/doiLink.cgi?JTE12507 [Accessed June 17, 2017].

Murphy, S. V., Skardal, A. & Atala, A., 2013. Evaluation of hydrogels for bio-printing applications. *Journal of Biomedical Materials Research Part A*, 101A(1), pp.272–284. Available at: http://doi.wiley.com/10.1002/jbm.a.34326 [Accessed December 29, 2016].

Murphy, S. V & Atala, A., 2014. 3D bioprinting of tissues and organs. *Nature Biotechnology*, 32(8), pp.773–785. Available at: http://www.nature.com/doifinder/10.1038/nbt.2958 [Accessed December 26, 2016].

Nawaz, Z. & Bentley, G., 2011. Surgical incisions and principles of wound healing. *Surgery (Oxford)*, 29(2), pp.59–62. Available at: http://linkinghub.elsevier.com/retrieve/pii/S0263931910002462 [Accessed June 29, 2017].

O'Meara, S. et al., 2000. Systematic reviews of wound care management: (3) antimicrobial agents for chronic wounds; (4) diabetic foot ulceration. *Health technology assessment (Winchester, England)*, 4(21), pp.1–237. Available at: http://www.ncbi.nlm.nih.gov/pubmed/11074391 [Accessed June 27, 2017].

Öztürk, E. et al., 2006. Preparation and characterization of ciprofloxacin-loaded alginate/chitosan sponge as a wound dressing material. *Journal of Applied Polymer Science*, 101(3), pp.1602–1609. Available at: http://doi.wiley.com/10.1002/app.23563 [Accessed June 30, 2017].

Pant, B. et al., 2012. Characterization and antibacterial properties of Ag NPs loaded nylon-6 nanocomposite prepared by one-step electrospinning process. *Colloids and Surfaces A: Physicochemical and Engineering Aspects*, 395, pp.94–99. Available at: http://linkinghub.elsevier.com/retrieve/pii/S0927775711007576 [Accessed June 26, 2017].

Park, M.V.D.Z. et al., 2011. The effect of particle size on the cytotoxicity, inflammation, developmental toxicity and genotoxicity of silver nanoparticles. *Biomaterials*, 32(36), pp.9810–9817. Available at: http://linkinghub.elsevier.com/retrieve/pii/S0142961211010337 [Accessed July 8, 2017].

Pawar, H.V., Tetteh, J. & Boateng, J.S., 2013. Preparation, optimisation and characterisation of novel wound healing film dressings loaded with streptomycin and diclofenac. *Colloids and Surfaces B: Biointerfaces*, 102, pp.102–110. Available at: http://linkinghub.elsevier.com/retrieve/pii/S0927776512004626 [Accessed June 30, 2017].

Pedde, R.D. et al., 2017. Emerging Biofabrication Strategies for Engineering Complex Tissue Constructs. *Advanced Materials*, 29(19), p.1606061. Available at: http://doi.wiley.com/10.1002/adma.201606061 [Accessed May 26, 2017].

Peppas, N.A. et al., 2006. Hydrogels in Biology and Medicine: From Molecular Principles to Bionanotechnology. *Advanced Materials*, 18(11), pp.1345–1360. Available at: http://doi.wiley.com/10.1002/adma.200501612 [Accessed July 16, 2017].

Queen, D. et al., 2004. A dressing history. *International Wound Journal*, 1(1), pp.59–77. Available at: http://doi.wiley.com/10.1111/j.1742-4801.2004.0009.x [Accessed July

13, 2017].
Queen, D. et al., 1987. The preclinical evaluation of the water vapour transmission rate through burn wound dressings. *Biomaterials*, 8(5), pp.367–71. Available at: http://www.ncbi.nlm.nih.gov/pubmed/3676423 [Accessed May 10, 2017].
Rees, A. et al., 2015. 3D Bioprinting of Carboxymethylated-Periodate Oxidized Nanocellulose Constructs for Wound Dressing Applications. *BioMed research international*, 2015, p.925757. Available at: http://www.ncbi.nlm.nih.gov/pubmed/26090461 [Accessed June 23, 2017].
Reynolds, P.E., 1989. Structure, biochemistry and mechanism of action of glycopeptide antibiotics. *European Journal of Clinical Microbiology & Infectious Diseases*, 8(11), pp.943–950. Available at: http://link.springer.com/10.1007/BF01967563 [Accessed June 26, 2017].
Schneider, L.A. et al., 2007. Influence of pH on wound-healing: a new perspective for wound-therapy? *Archives of Dermatological Research*, 298(9), pp.413–420. Available at: http://link.springer.com/10.1007/s00403-006-0713-x [Accessed June 27, 2017].
Schultz, G., 1999. Molecular regulation of wound healing. *Acute and chronic wounds: Nursing management. 2nd*.
Sharp, D. et al., 2010. Approaching intelligent infection diagnostics: Carbon fibre sensor for electrochemical pyocyanin detection. *Bioelectrochemistry*, 77(2), pp.114–119. Available at: http://linkinghub.elsevier.com/retrieve/pii/S1567539409001352 [Accessed June 27, 2017].
Sharp, D., Forsythe, S. & Davis, J., 2008. Carbon Fibre Composites: Integrated Electrochemical Sensors for Wound Management. *The Journal of Biochemistry*, 144(1), pp.87–93. Available at: https://academic.oup.com/jb/article-lookup/doi/10.1093/jb/mvn045 [Accessed June 27, 2017].
Shi, L. et al., 2011. pH in the Bacteria-Contaminated Wound and Its Impact on Clostridium histolyticum Collagenase Activity. *Journal of Wound, Ostomy and Continence Nursing*, 38(5), pp.514–521. Available at: http://content.wkhealth.com/linkback/openurl?sid=WKPTLP:landingpage&an=00152192-201109000-00008 [Accessed June 27, 2017].
Shupp, J.W. et al., 2010. Epidemiology of Bloodstream Infections in Burn-Injured Patients: A Review of the National Burn Repository. *Journal of Burn Care & Research*, 31(4), pp.521–528. Available at: http://www.ncbi.nlm.nih.gov/pubmed/20616647 [Accessed June 26, 2017].
Silver, S. et al., 2003. Bacterial silver resistance: molecular biology and uses and misuses of silver compounds. *FEMS Microbiology Reviews*, 27(2–3), pp.341–353. Available at: https://academic.oup.com/femsre/article-lookup/doi/10.1016/S0168-6445(03)00047-0 [Accessed July 8, 2017].
Slaughter, B. V. et al., 2009. Hydrogels in Regenerative Medicine. *Advanced Materials*, 21(32–33), pp.3307–3329. Available at: http://doi.wiley.com/10.1002/adma.200802106 [Accessed June 25, 2017].
Sridhar, V. & Takahata, K., 2009. A hydrogel-based passive wireless sensor using a flex-circuit inductive transducer. *Sensors and Actuators A: Physical*, 155(1), pp.58–65. Available at: http://linkinghub.elsevier.com/retrieve/pii/S0924424709003550 [Accessed June 28, 2017].

Srinivasan, K. & Mahadevan, R., 2010. Characterization of proton production and consumption associated with microbial metabolism. *biotechnology*. Available at: https://bmcbiotechnol.biomedcentral.com/articles/10.1186/1472-6750-10-2 [Accessed June 27, 2017].

Stinner, D.J. et al., 2010. Local Antibiotic Delivery Using Tailorable Chitosan Sponges: The Future of Infection Control? *J Orthop Trauma*, 24, pp.592–597. Available at: https://insights.ovid.com/pubmed?pmid=20736801 [Accessed June 25, 2017].

Sung, J.H. et al., 2010. Gel characterisation and in vivo evaluation of minocycline-loaded wound dressing with enhanced wound healing using polyvinyl alcohol and chitosan. *International Journal of Pharmaceutics*, 392(1–2), pp.232–240. Available at: http://linkinghub.elsevier.com/retrieve/pii/S0378517310001985 [Accessed June 30, 2017].

Tamayol, A. et al., 2016. Flexible pH-Sensing Hydrogel Fibers for Epidermal Applications. *Advanced Healthcare Materials*, 5(6), pp.711–719.

Temenoff, J.S. & Mikos, A.G., 2008. *Biomaterials : the Intersection of biology and materials science*, Pearson/Prentice Hall.

Thu, H.-E., Zulfakar, M.H. & Ng, S.-F., 2012. Alginate based bilayer hydrocolloid films as potential slow-release modern wound dressing. *International Journal of Pharmaceutics*, 434(1), pp.375–383. Available at: http://www.sciencedirect.com/science/article/pii/S0378517312005443 [Accessed May 10, 2017].

Unnithan, A.R. et al., 2012. Wound-dressing materials with antibacterial activity from electrospun polyurethane?dextran nanofiber mats containing ciprofloxacin HCl. *Carbohydrate Polymers*, 90(4), pp.1786–1793. Available at: http://linkinghub.elsevier.com/retrieve/pii/S0144861712007448 [Accessed June 30, 2017].

Wang, L. et al., 2002. Chitosan-alginate PEC membrane as a wound dressing: Assessment of incisional wound healing. *Journal of Biomedical Materials Research*, 63(5), pp.610–618. Available at: http://doi.wiley.com/10.1002/jbm.10382 [Accessed May 10, 2017].

Williams, R.L. et al., 1986. *Clinical materials.*, Edward Arnold. Available at: https://cwru.pure.elsevier.com/en/publications/the-biocompatibility-of-silver-2 [Accessed June 26, 2017].

Woodcock, J. et al., 1998. Interaction of antibiotics with A- and P-site-specific bases in 16S ribosomal RNA. *The EMBO journal*, 10(10), pp.3099–103. Available at: http://www.ncbi.nlm.nih.gov/pubmed/1915283 [Accessed July 3, 2017].

Zlotogorski, A., 1987. Distribution of skin surface pH on the forehead and cheek of adults. *Archives of Dermatological Research*, 279(6), pp.398–401. Available at: http://link.springer.com/10.1007/BF00412626 [Accessed June 27, 2017].

Zopf, D.A. et al., 2013. Bioresorbable Airway Splint Created with a Three-Dimensional Printer. *New England Journal of Medicine*, 368(21), pp.2043–2045. Available at: http://www.ncbi.nlm.nih.gov/pubmed/23697530 [Accessed June 23, 2017].